

Piezoelectric Nanogenerator Based on Lead-Free perovskite Embedded PVDF Composite for Biomechanical Energy Harvesting Application

*A thesis submitted towards partial fulfilment
of the requirements for the degree of*

Master of Technology in Nano science and Technology

Submitted by

Mrinmoy Patra

ROLL NO.: M4NST22018

REG. NO.:154587

Prof. (Dr). Kalyan Kumar Chattopadhyay

Head of The Department

Department of Physics

Jadavpur University

Kolkata -700032

Course affiliated to

Faculty Council of Interdisciplinary Studies,

Law and Management, Jadavpur university

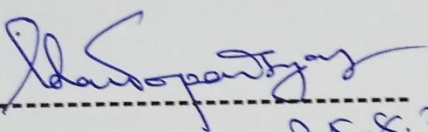
Kolkata-700032

India

M.Tech. (Nanoscience and Technology)
course affiliated
to Faculty Council of Interdisciplinary
Studies, Law and Management
Jadavpur University
Kolkata, India

CERTIFICATE OF RECOMMENDATION

This is to certify that the thesis entitled "Piezoelectric Nanogenerator Based on Lead Free Perovskite Embedded PVDF Composite for Biomechanical Energy Harvesting Application" is a bonafide work carried out by MRINMOY PATRA under our supervision and guidance for partial fulfilment of the requirement of Master of Technology in Nanoscience and Technology in School of Materials Science and Nanotechnology during the academic session 2020-2022.

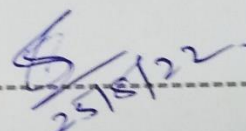

25.8.22

THESIS ADVISOR

Dr. Kalyan Kumar Chattopadhyay
Head of The Department
Department of Physics
Jadavpur University,
Kolkata-700032.



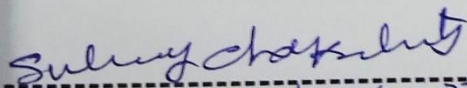
Prof. Kalyan Kr. Chattopadhyay
Professor and Head
Department of Physics
Jadavpur University
Kolkata - 700 032


25/8/22

DIRECTOR

Dr. Sourav Sarkar
Director
School of Materials Science
and Nanotechnology
Jadavpur University,
Kolkata-700032.

Dr. Sourav Sarkar
Director
Associate Professor
School of Materials Science & Nanotechnology
Jadavpur University
Kolkata - 700032


25/08/2022

DEAN

Subenoy Chakraborty
Faculty Council of
Interdisciplinary Studies, Law
and Management
Jadavpur University,
Kolkata-700032.

Dean
Faculty of Interdisciplinary Studies
Law & Management
Jadavpur University, Kolkata-700032

M.Tech.(Nano science and Technology) course affiliated to
Faculty Council of Interdisciplinary Studies, Law and Management
Jadavpur University
Kolkata, India

CERTIFICATE OF APPROVAL **

This foregoing thesis is hereby approved as a credible study of an engineering subject carried out and presented in a manner satisfactorily to warranty its acceptance as a prerequisite to the degree for which it has been submitted. It is understood that by this approval the undersigned do not endorse or approve any statement made or opinion expressed or conclusion drawn therein but approve the thesis only for purpose for which it has been submitted.

Committee of final examination

for evaluation of Thesis

** Only in case the thesis is approved.

DECLARATION OF ORIGINALITY AND COMPLIANCE OF
ACADEMIC ETHICS

I hereby declare that this thesis contains literature survey and original research work by the undersigned candidate, as part of his **Master of Technology (Nano science and Technology)** studies during academic session **2020-2022**.

All information in this document has been obtained and presented in accordance with academic rules and ethical conduct.

I also declare that, as required by this rules and conduct, I have fully cited and referred all material and results that are not original to this work.

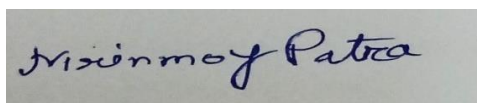
NAME: MRINMOY PATRA

ROLL NUMBER: M4NST22018

REG. NUMBER: 154587

THESIS TITLE: Piezoelectric nanogenerator based on lead free perovskite embedded PVDF composite for biomechanical energy harvesting application.

SIGNATURE:

A rectangular box containing a handwritten signature in blue ink that reads "Mrinmoy Patra".

DATE:25-08-2022

Acknowledgement

In the first place, I would like to express my profound gratitude to my supervisor **Prof (Dr). Kalyan Kumar Chattopadhyay** for his advice and guidance from the very early stage of this research as well as giving me extraordinary experiences throughout the work. Above all and the most needed, he provided me constant encouragement and support in various ways. Thank you also for the amicable environment conducive to extensive research work at Thin Film and Nanoscience Lab, in which you have welcomed me. All these provided me great support, helping me to confront the difficult periods of my project, which I do not think I would have completed it otherwise.

I want to extend my gratitude to my co-supervisor **Suvankar Mondal** (CSIR fellow, Jadavpur university) for his advices, guidance, and crucial contribution throughout my work. His involvement with his originality has triggered and nurtured my scholarly development that I will benefit from, for along time to come. I really cannot value his support and generous cooperation. He has been like an elder brother to me always by my side whenever needed him.

I would also like to express my sincere thanks to Prof. Sourav Sarkar, Prof. C.K. Ghosh, Dr. Mahua Ghosh Chowdhury for their help, support, encouragement, suggestion and advice during the course of the research. Their enthusiasm provided me a helpful and effective way of learning which in turn inspired me to follow the research project with great enthusiasm.

I would also really like to thank all the staff members of School of Materials Science and Nanotechnology and Department of Physics for carrying out the critical characterization parts of the synthesized samples that composed a very important part of the thesis.

I extend my heartiest thanks to all my seniors of 'Thin Film & Nano Science' lab especially Suvankar Poddar da, Pulak da, Moumita di, Sudip da, Riyaz da, Dimitra di, Ratna di, Biswajit da, Antika di, and everyone in this lab for extending their helping hands. I would also like to thank all my friends Saswata, Avinash, Tanay, Manas, Imran, Kamalesh and all of them for their encouragement and cooperation.

Finally, I express my special gratitude to my parents and all my well-wishers for their wholehearted support, love and encouragement.

Abstract

This study of the thesis work has been conducted with an objective to develop concepts and knowledge about perovskite-based material for energy harvesting application. Here we have studied some previous work on this topic. We have gone through the history, basic working principle, properties and what could be the possible future of this technology. In the course of literature surveying there are some research paper, scientific journals have been studied to develop ideas on different types of perovskite materials available having good electrical, chemical and optoelectronics properties. Exploited with the merits of easy congregation, conformal structure, flexible and self-powered piezoelectric nanogenerators (PENGs) have become a sustainable and attainable energy alternative. Following this trend, a novel piezoelectric sensor is fabricated by a composite of room temperature processed all-inorganic cesium antimony bismuth chloride ($\text{Cs}_3\text{SbBiCl}_9$) layered perovskite and polyvinylidene fluoride (PVDF) nanofiber. Studies on this novel material have already indicated its high electrical conductivity and tunable bandgap claiming the same as one of the promising materials for “piezo electronics”. Hence, we have selected this novel perovskite for this thesis work and focused on colloidal synthesis technique, investigation of its different physical and electrical properties, device fabrication and several interesting applications.

We started from the cost-effective chemical technique “colloidal” route to synthesize $\text{Cs}_3\text{SbBiCl}_9$. We had selected this synthesis route as it requires simple experimental set-up, minimum production cost compared to other techniques. From the Industrial application point of view large scale production for proper use of any advanced material is achievable. So, colloidal synthesis technique also fulfils these criteria. Moreover, several synthesis parameters like doping concentration, temperature and synthesis duration can be controlled efficiently. So, we opted for colloidal synthesis in our work.

Characterization of the synthesized samples was done with X-ray diffractometer (XRD) for phase information. Field emission scanning electron microscopic (FESEM) studies were carried out to obtain the morphology of $\text{Cs}_3\text{SbBiCl}_9$ samples. FTIR spectroscopy studies were carried out to investigate the electroactive phase content of the material. Detailed studies were performed using LCR meter to observe the nature of dielectric and ferro electric properties like piezoelectricity which is an important aspect of our material.

Piezoelectric energy generation from the devices has been investigated under several simple human body movements like hammering by hand, finger tapping, knee bending, bending by arm, etc. Optimized $\text{Cs}_3\text{SbBiCl}_9$ -PVDF composite (with 5 wt% of $\text{Cs}_3\text{SbBiCl}_9$ loading) based PENG delivered an output power 4.22 mW with high open-circuit voltage of 273 V and short-circuit current of 15.45 μA . Such promising output value for the composite sample suggests much improved energy conversion efficiency as compared to the pristine PVDF separately.

This device is also capable of lighting up several commercial LEDs. Increase in output values is attributed to the improved polarization in PVDF by $\text{Cs}_3\text{SbBiCl}_9$ incorporation. Furthermore, photosensitivity has been indicated in other journals, which designated its potential as photodetector. Considering the photo and electroactive properties, a new class of self-powered photoactive piezoelectric energy harvester has also been fabricated. Such results culminate the practical design of all inorganic perovskite-based nanostructure in optimizing device performance and thereby providing a useful way to develop new hybrid materials for piezo-phototronics.

Contents

Acknowledgement	i
------------------------	----------

Abstract	ii
-----------------	-----------

Chapter 1: Introduction and Objective:

1.1.	Nanostructure and Nanotechnology	7
1.2.	Properties of Nanomaterial	12
1.2.1.	Dielectric properties	13
1.2.2.	Ferroelectricity	13
1.2.3.	Piezoelectricity	14
1.2.4.	Electrical conductivity	15
1.3.	Applications	15
1.3.1.	Sensors	16
1.3.2.	catalyst	16
1.3.3.	Fuel cells and batteries	17
1.3.4.	Piezoelectric energy harvester	
1.4.	Introduction to all organic-inorganic perovskite	17
1.5.	Structure of halide perovskite	20
1.6.	Introduction of Cesium antimony bismuth chloride ($\text{Cs}_3\text{SbBiCl}_9$)	21
1.6.1.	Properties	23
1.6.2.	Structural analysis	24
1.6.3.	Perovskite-polymer (PVDF) composite	25
1.7.	Objectives	26

Reference

Chapter 2: Literature review of past work:	29
---	-----------

Reference	21
-----------	----

Chapter 3: Instruments and apparatus:

3.1.	Crystal structure analysis	40
3.1.1.	X-ray Diffractometer	41
3.2.	Optical property analysis	45
3.2.1.	Ultraviolet Visible spectrophotometer	46
3.3.	Morphological analysis	48
3.3.1	Field Emission Scanning Electron Microscope (FESEM)	49
3.3.2	Energy Dispersive X-ray analysis (EDAX)	53
3.4.	Analysis of absorbance spectra and molecular vibrations	54
3.4.1.	Fourier Transform Infrared Spectroscope (FTIR)	34
3.5	Electrical quantity analysis	57
3.5.1.	Measurements by Cathode ray Oscilloscope	58
3.6.	Surface characterization analysis	65
3.6.1.	X- ray photo electron spectroscopy	67
3.7	Measurement of dielectric property by impedance analyzer	68
3.7.1	Measurement of dielectric constant and dielectric loss	70

Chapter 4: Colloidal synthesis and characterization of Cs₃SbBiCl₉ perovskite:

4.1.	Introduction	73
4.2.	Experimental details	74
4.2.1.	Synthesis	74
4.2.2.	Characterization	75
4.3	Result and Discussion	76
4.3.1	Structural and Compositional studies	76
4.3.2.	Morphological studies	78
4.4	Conclusion	80

Reference	81
-----------	----

Chapter 5: Cs₃SbBiCl₉ and PVDF composite thin film preparation, characterization:

	Introduction	83
5.1.	Experimental details	84
5.2.	Result and discussion	85
5.2.1.	Structural analysis by XRD	85
5.2.2.	Morphological analysis by FESEM	86
5.2.3.	Electroactive β phase analysis by FTIR	87
5.2.4.	Dielectric measurement analysis by impedance analyzer	89
5.3.	Conclusion	91
	Reference	92

Chapter 6 Device fabrication of composite thin films, subjected to different bio-mechanical movements, results:

6.1.	Introduction	94
6.2.	Experimental details	95
6.2.1.	Device fabrication	95
6.3.	Result and discussion	96
6.3.1.	Analysis of different electrical parameters	96
6.3.2.	Analysis of different bio-mechanical movements	99
	Reference	102

Chapter 7 Conclusion and scope for future work:

7.1.	Conclusion	104
7.2.	Scope for future work	105

Chapter 1

Introduction and Objective

1.1 Nanostructures and nanotechnology

Nanoscience and nanotechnology are the study and application of exceedingly small things, which can be used in all the other science fields, such as biology, physics, chemistry and materials science. The word ‘Nano’ means one billionth of a meter” (From the talk **There’s Plenty of Room at the Bottom**, delivered by Richard P. Feynman at the annual meeting of the American Physical Society).

The concept of nanotechnology was first coined by the eminent physicist Richard Feynman in 1959 in his lecture which was published in 1960 enfranchised ‘There's Plenty of Room at the Bottom’ [1]. The term ‘nano-technology’ was first used by Norio Taniguchi in 1974 although it is not very well known to people since centuries. In 1986 inspired by Feynman’s concept, K. Eric Drexler used the word ‘nanotechnology’ in book ‘Engines of Creation: The Coming Era of Nanotechnology’[2].

Nanoscience is the science of objects with typical sizes of 1-100 nm at least in one direction. If matter is divided into such small objects the mechanical, electric, optical, and magnetic properties can be altered [3]. Bulk properties would diminish and nano properties would dominate. Quantum effects due to the size limitation come into play. Nanoscience and Nanotechnology are interdisciplinary topic, crossing the boundaries between physics, chemistry, chemical, electrical, mechanical, and electronics engineering.

Nanoscience considered to be is one of the most important developments in the last decades. New technologies were required to enter the nanoscale because many of the traditional Newtonian physics do not work at the nanoscale. The relationship between nanoscience and technology is like a symbiosis. Scientific discoveries lead to new technologies and eventually into implementations. Two new technologies which enabled the progress of nanoscience are scanning tunnelling (STM) and scanning force microscopy (SFM). They allow to image of

structure and manipulate objects on surfaces with enough precision even in ambient conditions or in liquids.

Nanotechnology refers any technology on a nanoscale that has applications in the real world. Nanotechnology encompasses the production and application of physical, chemical, and biological systems at scales starting from individual atoms or molecules to submicron dimensions, as well as the integration of the resulting nanostructures into larger systems. Nano technology is likely to have a profound impact on our economy and society in the early 21st century, comparable to that of semiconductor technology, information technology or, molecular biology. Science and technology research in nanotechnology promises breakthroughs in areas such as materials and manufacturing, nanoelectronics, medicine and healthcare, energy, biotechnology, information technology, and national security. It is widely felt that nanotechnology will be the next Industrial Revolution.

In the past few decades nanoscience and nanotechnology has been developed explosively due to discovery of novel synthesis routes and characterization techniques. There are various types of nanoscale structures like, nanotubes, nanowires, nanosheets etc. Nanoparticles are often called as quantum dots and can be considered as zero dimensional systems. It is nothing but basic physics acting behind the novel properties of the above systems and it has been well explained by quantum mechanical point of view. In order to understand these systems, it is very essential to discuss the density of states (DOS) of quantum dots (0 dimension), quantum wires (1 dimension) and quantum wells (2 dimensions) in brief.

The available electron states in a system can be calculated by the well-known Schrodinger's equation: $\mathbf{H}\psi = \mathbf{E}\psi$. Solving this we can finally get the density of states in k-space/ volume. In generalized form,

$$g(E) dE \approx E^{(d/2)-1}$$

Here, d is the dimensionality, and the energy is measured from the top of the valence band for holes and from the bottom of the conduction band for electrons. In the 3D system, $g(E)$ is a smooth square-root function of energy. In case of 2D system, $g(E)$ is constant, therefore drastically changed from 3-D case. In 2-D system the energy spectrum is quasi-continuous, but the density of states is step function [10]. Every time when we go to a lower dimensionality system, the dependency of DOS on energy changes by $E^{-1/2}$.

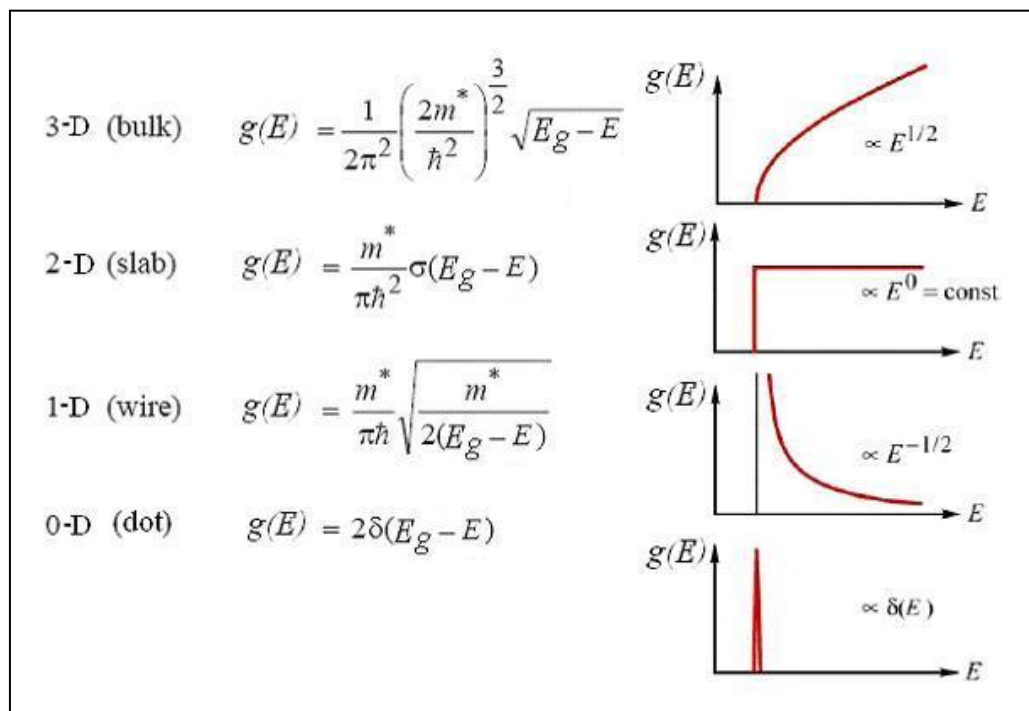
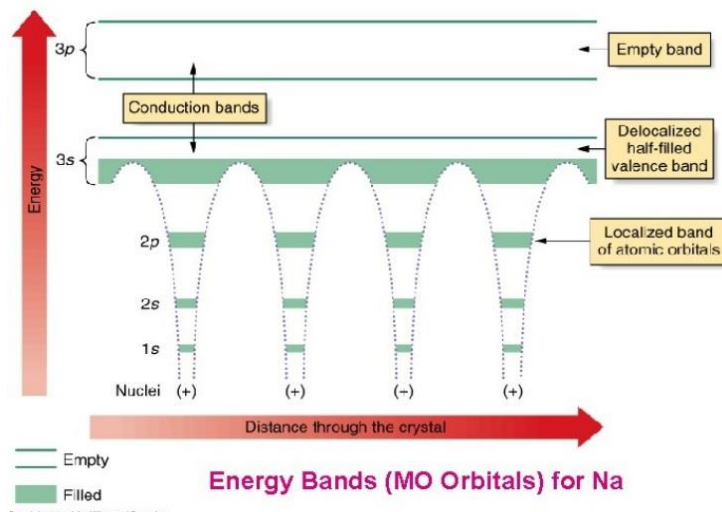


Fig.- Schematic illustration of structural dimensionality of materials with density of states.

Now the “quantum size effect” should be discussed in brief. For this effect the electronic properties of materials are changed with pronounced reduction of its particle sizes. This effect does not play any role if the reduction of dimension is confined from macro to micro. Conversely, in the nanoscale, quantum effect becomes very prominent. When the sizes of the nanoparticles are equivalent to that of Bohr excitonic radius (r_B) of those materials quantum confinement effect modifies the electronic structure of nanocrystals. If particle radius (r) in the

nanocrystalline materials are less than Bohr radius ($r < r_B$), strong quantum confinement effects take place. Weak quantum confinement effects are found within particles having radius larger than Bohr radius ($r > r_B$).

Property of solids vary widely as their ability to conduct current and we can see this by the difference in resistivity between good conductor and insulator. The electrical resistivity of pure metal is about 10^{-12} ohm-cm at 1K temperature. The resistivity of a good insulator is as high as 10^{22} ohm-cm and can be widest up to 10^{32} ohm-cm. The existence of electron band energy in solids makes it possible to understand this remarkable range [4].



Above picture shows the band theory of solids. It is seen that the energy bands are formed from the overlap of atomic orbitals of similar energy from all atoms in solids. Energy bands having core electrons (non-valence) are localized and energy bands having valence electrons are delocalized. If we solve the time independent Schrodinger equation, we get, change in energy level

$$E_2 - E_1 = \Delta E = \frac{h^2 \pi^2 (n_2^2 - n_1^2)}{2mL^2}$$

$n = 1, 2, 3, \dots$, m = mass of the particle, L = dimension of particle, h = Plank's constant

So, we can say a few things from this equation that, the change in energy levels from one state to another is inversely proportional to the square of the dimension of particle. 1. This means as we move towards bulk to nano scale the energy difference between two levels increases. 2. It is seen that different energy levels of microscopic particles are ‘quantized’. 3. Also, the energy level increases as the mass of the system decreases.

Metals contain a band that is partly empty and partly filled regardless of temperature. Therefore, they have very high conductivity. The lowermost, almost fully occupied band in an insulator or semiconductor is called the valence band by analogy with the valence electrons of individual atoms. The uppermost, almost unoccupied band is called the conduction band because only when electrons are excited to the conduction band can current flow in these materials. The difference between insulators and semiconductors is only that the forbidden band gap between the valence band and conduction band is larger in an insulator, so that fewer electrons are found there and the electrical conductivity is lower. Because one of the main mechanisms for electrons to be excited to the conduction band is due to thermal energy, the conductivity of semiconductors is strongly dependent on the temperature of the material. Fermi energy concept have been discussed by *Coons* in the term project [5].

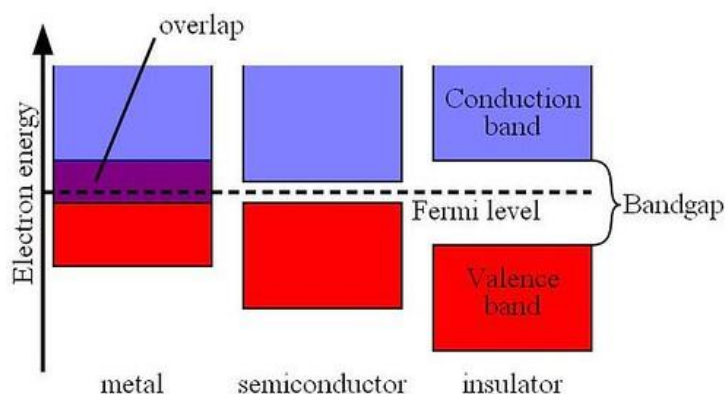


Fig.- Simplified diagram of the electronic band structure of metals, semiconductors, and insulators.

This band gap is one of the most useful aspects of the band structure, as it strongly influences the electrical and optical properties of the material. Electrons can transfer from one band to the other by means of carrier generation and recombination processes. The band gap and defect states created in the band gap by doping can be used to create semiconductor devices such as solar cells, diodes, transistors, laser diodes, and others [6].

1.2 Properties of Nanomaterial

1.2.1 Dielectric properties

Dielectrics can be defined as materials that are very poor conductors of electric current. They are insulators and contain no free electron. Dielectrics can be easily polarized when an electric field is applied to it. Therefore, their behavior in an electric field is entirely different from that of conductors. Dielectric materials are the materials in which electro-static fields can conserve for a long time (Guangda et al. [7]). It showed a great resistance to electric current channel below the action of the applied direct current voltage and diverge sharply in their simple electrical properties from conductive materials. Layers of these materials are generally inserted into capacitors to improve their performance, and the term dielectric refers to this application. Good dielectric permittivity or ferroelectric materials are of massive importance as electro-ceramics for engineering and electronics industry. Ferro-electricity is generally described by a soft-mode model (Sebastian et al. [8]). Several routes have been pursued to explain the dielectric and mechanical properties starting from the simple structure BaTiO_3 by the solid solution system $\text{Pb}(\text{Zr,Ti})\text{O}_3$ to other distinct families of materials.

1.2.2 Ferroelectricity

A ferroelectric crystal exhibits an electric dipole moment even in the absence of an external electric field. In this state the center of positive charge does not coincide with the center of negative charge (Charles kittel et al. [9]). Ferroelectricity is the phenomenon that occurs when an external electric field is applied to some materials leading to a spontaneous electric polarization (Retot et al. [10]). The discovery of ferroelectricity in perovskite-based materials (Qingteng, 2012) and other barium titanate (BaTiO_3) opened up new application for ferroelectric materials, leading to significant interest in other types of ferroelectrics (Eman Abdul Rahman Assirey et al. [11]). The ferroelectric materials have dielectric constant two times larger in magnitude than those in ordinary dielectric. BaTiO_3 is a well-known

ferroelectric material with relative dielectric constant, its crystal at room temperature, exhibits no net polarization, in the absence of an external field, even though the dipoles of adjacent unit cells are aligned.

1.2.3 Piezoelectricity

All the crystals in ferroelectric state are also piezoelectric; say a stress Z is applied to the crystal will change the electric polarization. Similarly, an electric field E applied to the crystal will cause the crystal to become strained. Piezoelectric equations are,

$P = Zd + E\chi$; $e = Zs + Ed$; where P is the polarization, Z is stress, E is the electric field, χ is dielectric susceptibility, e the elastic strain and s is elastic compliance constant, d is the piezoelectric strain constant. Some materials have the capacity to produce an electric charge in reaction to applied mechanical stress is known as Piezoelectricity (Wang et al. [12]). Therefore, if definite crystals were subjected to mechanical strain, they became polarized at a degree which is proportional to the applied strain. On the other hand, they have some changed when they were exposed to an electric field which is known as the inverse piezoelectric effect. There is a difference between piezoelectric and ferroelectric materials, in the first materials it requires some external impetus while in the second there is spontaneous alignment of electric dipoles by their mutual interaction. Therefore, all piezoelectric are not ferroelectric but all ferroelectrics are piezoelectric (Gregor et al. [13]).

1.1.4 Electrical conductivity

The Charge transport phenomenon for materials with nanoscale dimension mainly depends on the grain boundary of a crystal [14] and also on the DOS of material. The effects of grain boundary plays a very significant role as its interface contains a density of defects like vacancies, dangling bonds, vacancy clusters etc [15]. Therefore, charge transport may occur by dipole re-orientation, electronic relaxation polarization and space charge distribution at

grain boundary interfaces in the presence of an external field. Upon external heating the grain boundary defects play important role to change the dielectric property of the material, hence the electrical conductivity changes.

1.3 Applications

1.3.1 Sensors

There are sum of requirements that the resources used as gas devices must have such as hydrothermal constancy, good similarity with the gases to be detect, suitable electronic configuration, resistance to poisoning, and alteration with existing skills. Perovskite oxides used as gas sensors like some semiconductors, LaFeO_3 , SrTiO_3 , $\text{CH}_3\text{NH}_3\text{PbI}_{3-x}(\text{SCN})_x$, $\text{CH}_3\text{NH}_3\text{PbI}_3$ They are interesting materials as gas sensors for their ideal band gap, thermal stability, and size difference between the cation sites. Perovskites materials which contain cobaltates, titanates, and ferrites were applied as gas sensors for spotting CO, NO₂, methanol, ethanol, and hydrocarbons (Taylor et al. [16]). Nanomaterials are often used as optical sensor for their excellent optoelectronic properties like, direct and tunable bandgaps, large absorption coefficients, broad absorption spectra, high carrier mobilities, and long carrier diffusion lengths. They are also being used as bio-mechanical sensors which will be discussed later on in this paper.

1.3.2 Catalyst

Perovskite oxides and halides used universally as catalyst in new chemical processing, showing suitable solid-state, surface, and morphological properties (Thirumalairajan et al. [17]). Several perovskites proved to have excellent catalytic activity to different reactions like hydrogen evolution, reduction reactions, and oxygen evolution. These nanomaterials have showed good photocatalytic and chemical catalytic property which made them versatile to be used as photodetector, active material for solar cells, and in therapeutic applications.

1.3.3 Fuel cells and batteries

In last few decades fuel cells are used as substitutes to combustion engines due to their possibility to reduce of the environmental pollution. They used specific type of chemical compound (nanomaterials) as dielectric medium which transfer to electrical energy like battery. Fuel cells are more acceptable for use due to their effectiveness, zero noise pollution, low emissions of toxic gases and its use in future hydrogen fuel economy. There are numbers of categories of fuel cells but solid oxide fuel cell are the greatest common samples of fuel cells (El-Ads et al. [18]). Nanomaterials rGO, several perovskites are optimized to be used as dielectric in modern days batteries and in super capacitors.

1.3.4 Piezoelectric energy harvester

These days, micro- or nano-scale integration of sensors, actuators, and circuits may permit more accurate diagnosis and more effective therapies for many diseases; similarly, wireless sensors networks can permit to drastically reduce the maintenance costs for structural health monitoring (buildings, bridges, highways, trains, airplanes) and help to prevent disasters. These are useful in making pressure sensors, self-powered devices like, nanogenerator. Biomechanical pressure enables this nanogenerators to generate voltage in its own. Gianni Ciofani et al. [19] described that despite these outstanding possibilities, the applications of both implantable micro- or nano-systems and wireless sensor networks are restricted by the limits of currently available batteries, which have insufficient energy density, adequate power density, do not guarantee sufficient lifetimes, may be not possible or too costly to replace. As a solution, since energy is, somehow, everywhere, it is possible in principle to harvest free energy from the environment; as an example, the human body is a great pool of energy, including: mechanical energy related to body movement and muscle contraction; hydraulic energy related to blood and other body fluid flow; chemical energy related to glucoses or other biomolecular energy sources and processes; and thermal energy related to body temperature. Similar considerations also apply to numerous other

environments. Moreover, even for very large-scale energy production with zero, or almost zero, environmental impact, it is in principle possible to harvest energy from the environment (solar energy, ocean waves, wind, geothermal, biomass...). As a result, the high-efficiency harvesting of energy from the environment is a key challenge for both large energy production and for the development of miniaturized self-powered devices with unlimited autonomy. Though energy harvesting devices may operate at macroscopic scale, in principle, operations at micro- or nano-scale can have decisive merits, especially for powering micro- and nano-devices, as necessary for both implantable MEMS, NEMS and wireless sensors networks.

1.4. Introduction to all organic-inorganic perovskite

The increase in energy crisis and global climate change have been addressed in two world summits namely Montreal protocol (1987) and Kyoto protocol (1997). The prime agenda of those summits was to protect the ozone layer from its rapid depletion, minimize the industrial emission, use of renewable source of energy to protect the environment.

One such candidate is perovskite material. Perovskite is a mineral found in Earth's mantle. It was first discovered by a German physicist Gustav Rose in 1839. Chemical composition that compound was CaTiO_3 . In recent years halide perovskites have been very popular due to its excellent optoelectronic properties and low cost. In 1978 organic inorganic halide perovskite was first synthesized and in 1994 researchers of IBM developed light emitting devices luminescent organic inorganic halide perovskite. In 1999 M Chikao et al. [20] fabricated an optical absorption layer in a solar cell by using rare-earth-based perovskite compound. Nowadays these perovskite materials are implemented in solar cells as photon absorbing active region.

Single Perovskite: This emerging technology of organic and inorganic perovskite has been implemented to improve their power conversion efficiency with inexpensive processing. The

most rapidly used perovskite is organic or inorganic lead perovskite. The general formula of a single perovskite is ABX_3 .

Where, A= monovalent organic or, inorganic cation

B= divalent metal cation

X= halide ion

Some examples of A in organic family are methyl ammonium (MA^+) with a chemical formula of CH_3NH_3 , formamidinium (FA^+) having a chemical formula of $[HC(CH_2)_2]^+$. Inorganic cations are Cs^+ , Rb^+ and so on. Examples of B are Pb^{+2} , Sn^{+2} . Examples of X are Cl^- , Br^- , I^- .

There are some promising perovskite materials showing good photovoltaic, optical absorption properties are as follows, $MAPbI_3$, $FAPbI_3$, $CsPbI_3$, $CsPbBr_3$, $CsSnI_3$.

Single perovskite shows an octahedral crystal orientation. Unit cell of octahedral perovskite has face, corner and center atoms in closed pack arrangement. Corner atoms consist with organic or inorganic metal cations, face atoms consist of halide ions and center atom consists of divalent metal cations. The figure below shows the octahedral crystal structure of single perovskite material.

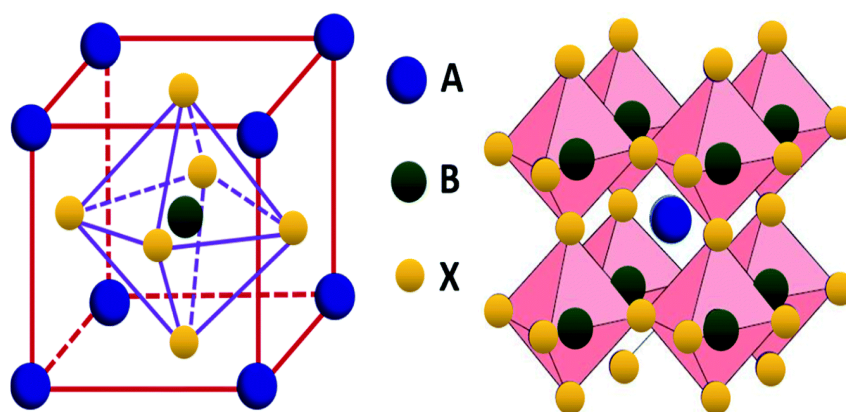


Fig. 1.1- Crystal structure of a single perovskite

Recent progress has been made to improve the performance of perovskite material. It has been predicted that an efficiency of more than 25% is achievable in the near future. In order to achieve that several modification techniques have been adopted.

Pb free perovskite:

- I. Lead is highly toxic and can cause serious damage.
- II. Pb based perovskite show excellent optoelectronic properties.
- III. It has high electron mobility.
- IV. High carrier diffusion length.
- V. It exhibits high charge carrier life time.
- VI. High absorption coefficient.
- VII. Narrow direct bandgap.

Despite of having several advantages Pb could still not be used commercially due its hazardous effect. Perhaps it has been substituted by some other divalent cation (like, Sn) or combination of monovalent and trivalent cations. Ag⁺ is a commonly used monovalent cation and Bi/ Sb used as trivalent. They are experimented and showed satisfactory result nearly close to Pb based perovskite. Some examples are Cs₂AgBiBr₆, RbAgBiBr₆

Double perovskite: In recent times, double perovskite materials have been emerged as one of the best alternatives of Pb based single perovskites. It shows good stability with moderate optical properties. The basic formula of crystal structure is ABB'X. Where,

A= Organic or inorganic monovalent cation (MA⁺, Cs⁺)

B= Monovalent metal cation(Ag⁺)

B'= Trivalent cation(Bi⁺³,Sb⁺³)

X= Halide ions

Double perovskite shows 3D octagonal crystal structure. It has good stability moderate performance and most importantly it is nontoxic.

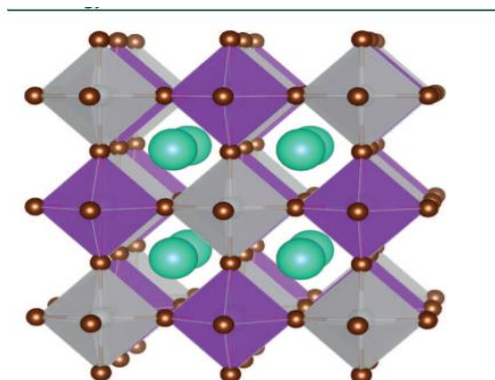


Fig. 1.2- Crystal structure of double perovskite material

1.5 Structure of Halide perovskite

Fundamentally there are two types of perovskite structure which are already been discussed earlier. Single perovskites may contain one monovalent cation (Cs, Rb, CH₃NH₃ etc.), one divalent metal cation (Pb, Sn, Cu etc.) and a monovalent anion (Cl, Br, I etc.). Double perovskites may contain a monovalent cation (Cs, Rb, CH₃NH₃ etc.), two trivalent metal cation (Bi, Sb etc.) and a monovalent anion (Cl, Br, I etc.). These monovalent cations can be organic or inorganic elements having their own merits and demerits.

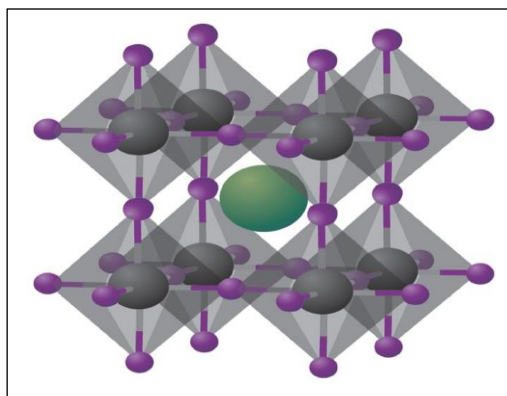


Fig. 1.3- Crystal structure of cubic metal halide perovskite with the chemical formula ABX_3 .

Organic or inorganic cations occupy position A (green) whereas metal cations and halides occupy the B (grey) and X (purple) positions, respectively.

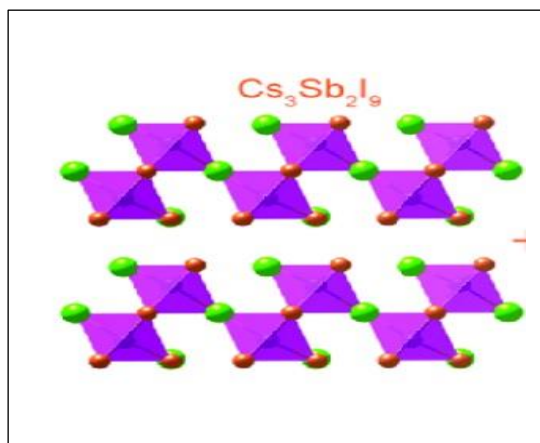


Fig. 1.4- Crystal structure of trigonal metal $\text{Cs}_3\text{Sb}_2\text{I}_9$ double perovskite. Organic or inorganic cations occupy position A (purple) whereas trivalent metal cation B, B' (red) and monovalent anion X (green) positions, respectively.

1.6 Introduction of Cesium antimony bismuth chloride ($\text{Cs}_3\text{SbBiCl}_9$)

All Organic-inorganic hybrid and inorganic lead halide perovskites are of intense research interest because of the large-range of optoelectronic applications (S.D Stranks et al. [21]). Methylammonium lead halide perovskites appeared as groundbreaking solar cell absorbers with comparable power conversion efficiency to that of traditional silicon solar cell materials. However, these compounds suffer drawback for practical application in large scale because of the toxicity (T. C Jellicoe et al. [22]) of lead as well as their poor stability towards light, heat, and atmospheric moisture. Thus, the development of an all-inorganic lead-free halide perovskite with improved photo-conversion efficiency is of utmost importance to solve the problem of instability and toxicity. Lead has been replaced by divalent cations like Sn^{2+} Ge^{2+} trivalent cations like Sb^{3+} , Bi^{3+} , one monovalent and one trivalent cation, tetravalent cations like Pd^{4+} and Sn^{4+} . Instead of three divalent cations (Pb^{2+}) in a halide perovskite ($\text{Cs}_3\text{Pb}_3\text{X}_9$; X = halide) two trivalent cations (M^{3+}) can be substituted and led to a defect perovskite of formula $\text{Cs}_3(\text{M}^{3+})_2\text{X}_9$. These kinds of substitution further lead to improve photovoltaic performance with an added advantage of choosing earth abundant and non-toxic elements. The

bulk phase synthesis of $(\text{CH}_3\text{NH}_3)_3\text{Sb}_2\text{I}_9$, $(\text{NH}_4)_3\text{Sb}_2\text{I}_x\text{Br}_{9-x}$ and $\text{Cs}_3\text{Sb}_2\text{I}_9$ are carried out earlier for the PV application. These materials could be further studied for the improvement in carrier migration, better light trapping capability, band gap tunability, enhanced photovoltaic efficiency as well as stability with the substitution of different elements at various sites of the material. $\text{Cs}_3\text{M}_2\text{X}_9$ ($\text{M} = \text{Sb, Bi}$; $\text{X} = \text{Cl, Br}$) perovskites exist in two different crystal structures, trigonal and orthorhombic. These lead-free halide perovskites contain MX_6 polyhedral, which are corner shared to form a layered structure in ab plane in trigonal phase while these form zigzag double chains running along b-direction in the orthorhombic phase. Recently, Pradhan et al. have synthesized mixture of trigonal and orthorhombic phases of $\text{Cs}_3\text{Sb}_2\text{Cl}_9$ nanocrystals by tuning the precursors and ligands. Yao et al. [23] have synthesized a series of $\text{A}_3\text{M}_2\text{X}_9$ ($\text{A} = \text{CH}_3\text{NH}_3, \text{Cs, Rb}$; $\text{M} = \text{Sb, Bi}$; $\text{X} = \text{Cl, Br, I}$) perovskite nanocrystals with Bi substitution at Sb site. However, a detailed study on the phase stability and the phase transition from trigonal to orthorhombic with substitution and temperature is lacking. Herein, we have reported the phase transition of bulk $\text{Cs}_3\text{Sb}_2\text{Cl}_9$ from trigonal to orthorhombic phase by substituting small amount of Bi at the Sb site as well as by varying reaction temperature. This structural change is confirmed from both powder X-ray diffraction and the room temperature Raman study. We were also able to tune the band gap by substitution of Bi at Sb site in $\text{Cs}_3\text{Sb}_2\text{Cl}_9$. The detailed structural, optical as well as the theoretical calculation were carried out.

1.6.1 Properties

- This double perovskite has high carrier mobility.
- High absorption coefficient.
- High carrier diffusion length.
- It shows poor stability under environmental exposure than Pb-based perovskite.

- Narrow direct band gap.
- High charge carrier life time.
- Less toxic than Pb-based perovskite.

1.6.2 Structural analysis

Atomic arrangements of $\text{Cs}_3\text{SbBiCl}_9$ of different elements are shown by the help of Rietveld refinement approach. Rietveld refinement is a technique described by Hugo Rietveld for use in the characterization of crystalline materials. The neutron and X-ray diffraction of powder sample results in a pattern characterized by reflections (peaks in intensity) at certain positions. The height, width and position of these reflections can be used to determine many aspects of the material's structure. Greenish blue atoms signify Cesium atoms, whereas, brown and green atoms signify Bismuth/ antimony and Chlorine atoms respectively.

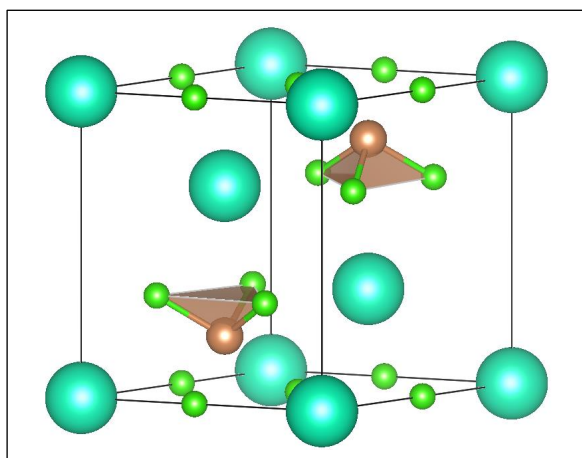


Fig. 1.5- Rietveld refinement structure of Cesium antimony bismuth chloride

1.6.3 Perovskite-polymer (PVDF) composite

In order to explain perovskite-polymer composite structure, one needs to know why it is necessary to mix these materials.

- **Polyvinylidene difluoride (PVDF)**

Polyvinylidene fluoride (PVDF) is a highly non-reactive thermoplastic fluoropolymer produced by the polymerization of vinylidene difluoride. PVDF has four crystalline phases, namely α , β , γ and δ depending on their chain conformation. Among them α is thermodynamically most stable and non-polar in nature. β and γ are polar phases. Non polar PVDF is used as insulator and painting. Polar PVDF is used in energy harvesting, sensor, electronics application. PVDF has several properties like bio-compatible, chemical resistance, good film forming capability, and it's cost effectiveness. Out of those four crystalline phase β is of utmost importance due to its spontaneous polarization and piezoelectric sensitivity (Binoy Bera et al. [24]).

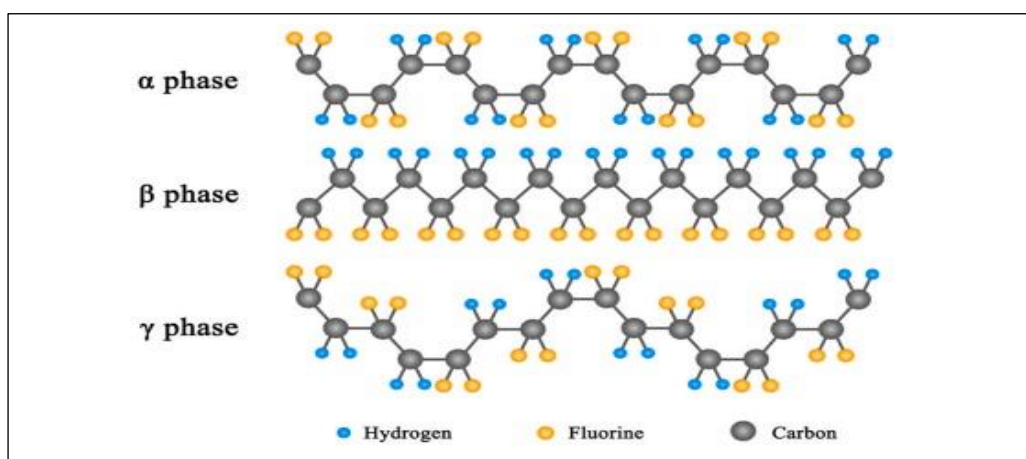


Fig. 1.6- Semicrystalline α , β , γ phase conformation of PVDF polymer.

- **Composite formation to enhance crystalline β phase**

Here it is needed to discuss that, tremendous effort has been given to induce electroactive β phase in PVDF. Several methods are there to enhance β phase in PVDF. It can be achieved by placing it into a high electric field which randomly orients CH_2/CF_2 dipoles along with the electrical field direction. Different types of doping (like metal nanoparticle, hydrated salt) also

done for achieving electroactive phase formation. Now a days PVDF is used in nanogenerator application due to its piezoelectricity property. PVDF is non-toxic, flexible, easy to process, makes it suitable for nanogenerator application. PVDF is a polymer material which shows piezoelectricity when external pressure or mechanical force applied on it. Piezoelectric material can be of crystals, ceramics or polymer. Piezoelectric crystals are like quartz, gallium orthophosphate, and tourmaline etc.

1.7 Objectives

The prime objectives of this thesis are to prepare $\text{Cs}_3\text{SbBiCl}_9$ double perovskite with a pure phase by colloidal route of synthesis and also to study various structural, morphological, electrochemical, electrical properties of that material. We would also study about perovskite-PVDF composite and thin film preparation.

Our specific objectives of the thesis are as follows

1. To synthesize pure phase of $\text{Cs}_3\text{SbBiCl}_9$ by a low-cost synthesis process like, colloidal synthesis route. To determine optimum synthesis condition by optimization of the synthesis parameter by developing a successful technology of pure $\text{Cs}_3\text{SbBiCl}_9$ is also an important factor.
2. Preparation of composite using PVDF and $\text{Cs}_3\text{SbBiCl}_9$ by colloidal route to make the composite nucleated properly. Thus, it could be used for thin film preparation to study piezoelectric property.
3. Also, we would characterize the synthesized samples by different sophisticated techniques like X-ray diffraction (XRD), Field emission scanning electron microscope (FESEM), Fourier transform infrared spectroscopy (FTIR), Dielectric measurement by LCR meter. These are some of the objectives of this thesis.
4. We would develop a very cost-effective device fabrication method, so that, it could be used

for bio-mechanical energy harvesting application.

5. Eventually, we find out some more significant applications using this composite thin film of PVDF and $\text{Cs}_3\text{SbBiCl}_9$ in the near future is also our motive.

References

- [1] R. P. Feynman, A lecture in engineering science, In California Institute of Technology, Feb. edn. 1960.
- [2] Drexler, K. Eric. Engines of creation. Anchor, 1986.
- [3] R. G. Gordon, MRS Bull. 25 (2000) 52
- [4] P. Motiarty, Rep. Prog. Phys. 64 (2001) 297.
- [5] Kuo-Feng Lin, Hsin-Ming Cheng, Hsu-Cheng Hsu, Li-Jiaun Lin, Wen-Feng Hsieh, Chemical Physics Letters 409 (2005) 208–211
- [6] O. Vigil, F. Cruz, A. Morales-Acevedob, G. Contreras-Puente, Materials Chemistry and Physics 68 (2001) 249–252 [13] G. Anil Kumar, M. V. Ramana Reddy, KattaNarasimha Reddy, Journal of Physics: Conference Series 365 (2012) 01203
- [14] H. Merzouk, A. Chelouche, S. Saoudi, D. Djouadi, A. Aksas, ApplPhys A (2012) 109:841–844
- [15] K. Aryal, B. N. Pantha, J. Li, J. Y. Lin, and H. X. Jiang, Applied Physics Letters 96, 052110 (2010)
- [16] Ryu Abe, Kazuhiro Sayama, and Hideki Sugihara, J. Phys. Chem. B 2005, 109, 16052–16061
- [17] O. Vigil, F. Cruz, A. Morales-Acevedob, G. Contreras-Puente, Materials Chemistry and Physics 68 (2001) 249–252 [13] G. Anil Kumar, M. V. Ramana Reddy, KattaNarasimha Reddy, Journal of Physics: Conference Series 365 (2012) 012031

- [18] Ludmila P. Oleksenko, Nelly P. Maksymovych, Evgeniy V. Sokovykh, Igor P. Matushko, Andrii I. Buvailo, Norman Dollahon, *Sensors and Actuators B* 196 (2014) 298–305
- [19] Genchi GG, Marino A, Rocca A, Mattoli V, Ciofani G. Barium titanate nanoparticles: promising multitasking vectors in nanomedicine. *Nanotechnology*. 2016 May 5;27(23):232001.
- [20] Li G, Rivarola FW, Davis NJ, Bai S, Jellicoe TC, de la Peña F, Hou S, Ducati C, Gao F, Friend RH, Greenham NC. Highly efficient perovskite nanocrystal light-emitting diodes enabled by a universal crosslinking method. *Advanced materials*. 2016 May;28(18):3528-34.
- [21] Stranks SD, Snaith HJ. Metal-halide perovskites for photovoltaic and light-emitting devices. *Nature nanotechnology*. 2015 May;10(5):391-402.
- [22] Yao H, Zhou F, Li Z, Ci Z, Ding L, Jin Z. Strategies for improving the stability of tin-based perovskite (ASnX_3) solar cells. *Advanced Science*. 2020 May;7(10):1903540.
- [23] Bera B, Sarkar MD. Piezoelectricity in PVDF and PVDF based piezoelectric nanogenerator: a concept. *IOSR J. Appl. Phys.* 2017;9(3):95-9.

Chapter-2

Literature review of past work

Environmental pollution due to chemical batteries, depletion of fossil energies are some major concerns. The group of Lijun Lu et al. [1] have shed light on the development of technologies in place of various portable electronic devices that are being used these days. In recent years piezoelectric nanogenerator is a worthy candidate due to easier fabrication method, longer working time, smaller in size, mechanical flexibility, environmental susceptibility and excellent energy harvesting capability. PVDF based flexible nanogenerators have been widely concerned and become a hot topic of research due to their strength and flexibility. There are wide range of applications like, self-powered energy source, which can replace chemical batteries, energy harvesting based on human motion, treatment of diseased organ by implementing micro medical devices etc. A PVDF based energy harvester was developed by T. Huang et al. [2] group which scavenged the heartbeat of a rat and charge a 4.7 μF capacitor to 0.5 V within 5 minutes. A study also showed movement of rats in vitro give an output voltage of 6 mV and current of 6 nA with PVDF-TrFF thin film, Various fabrication techniques such as spin coating, electrospinning have also been discussed here.

Jie Yang et al. [3] reported the prospects for harvesting mechanical energy and powering electronic devices using polymer based nanogenerators. In this study graphene oxide (GO) is added into PVDF to make a nanofiber mat by electrospinning method. Adding of GO enhances the β -phase content of PVDF. It gives a short-circuit current of 200 nA and the open-circuit voltage of 1.5 V. Reduced graphene oxide (rGO) was obtained by reducing the temperature to 140 °C gives a further increase in the electroactive β -phase content of PVDF. Hence a short-circuit current and open-circuit voltage of 700 nA and 16 V respectively were obtained due to high electrical conductivity of rGO. Shi et al. [4] fabricated the barium titanate (BT), graphene nanosheets and PVDF composites which showed a significant increase in the β -phase content. Some other nanofillers such as zinc-oxide (ZnO) nanoparticles (NPs), multiwall-carbon

nanotubes (MW-CNTs) can also be used according to this study. The diameter distributions of pure PVDF, GO/PVDF and rGO/PVDF fibers were 0.15~0.35 μm , 0.1~0.25 μm and 0.1~0.25 μm , respectively. Compare to pure PVDF fiber, the diameter of the composite fiber was decreased due to addition of GO and rGO, which enhanced the electrical conductivity of the electrospinning solution. So the study showed how GO nanofiller can increase the electrical conductive and decrease the fiber diameter significantly.

Ran Ding et al. [5] emphasized their study on hybrid organic-inorganic halide perovskite, which attracted massive attention for researchers. The ferroic nature of hybrid perovskite, such as ferroelectric and piezoelectric properties have been showing promising opportunities for mechanical energy harvesting application. Some of the piezoelectric materials such as zinc oxide (ZnO), barium titanate (BaTiO_3), lead zirconate titanate (PZT), polyvinylidene difluoride (PVDF) etc have been into picture. Some organic monovalent cations like methyleammonium (MA), formamidinium(FA) are used in place of inorganic cations like Cs, Rb etc. Nowadays a combination of both organic and inorganic perovskites have been coming forward since a wide range of applications because of their advantageous properties, such as tunable bandgap, superior charge transporting, and low-temperature processing, diverse compositions. This study also shows how TENG and PENGs are playing a vital role in mechanical energy harvesting application. Controlling the ferroelectric properties via compositional and structural engineering provide a good base for designing high temperature perovskite ferroelectrics with high saturation polarization Stability issues of hybrid perovskites, especially moisture sensitivity and thermal stability, still remain a concern in their practical applications. Although the ambient stability has been improved by developing 2D perovskites, but the intrinsic properties of those perovskites are still a challenge compared to the traditional oxide perovskites.

The highly toxic Pb based perovskites have not been commercialised due to hazardous effects. Weijun Ke et al. [6] demonstrated that Pb has been substituted by other halides like, Sn, Ge and so on. Pb has excellent opto electronics properties like, high optical absorption, low exciton binding energy, narrow direct band gap, high charge carrier mobility. Efficiency of Pb based perovskites have reached to 23.7% out performing Cu (Ga/In) (Se,S)₂ and Si based solar cells. But unfortunately, it is toxic and has a poor stability. Organic monovalent cations such as methyleammonium(MA), formamidinium (FA) and inorganic monovalent cations like Cs, Rb are being used with highly stable Sn⁴⁺ oxidation state instead of Sn²⁺ which is not stable in the atmosphere. MASnI₃, FASnI₃, CsSnI₃ have direct band gap of 1.2, 1.41 and 1.3 eV respectively. Apart from Sn and Pd based perovskite double perovskite has been studied. It has a crystal structure of A₂M⁺M³⁺X₆. These are 3D materials exhibit wider band gap of 2 eV, have good stability in air but show indirect band gap. Example of such material is CS₂AgBiBr₆. Despite Cs₂SnI₆ having a good stability, it has low mobility, too high minority carrier recombination lead to poor performance. Future progress is made in expanding carrier diffusion length by making high quality grains and less defects. Ge though is not suitable as it has high cost. Sn²⁺ based perovskite shows high efficiency but poor stability when subjected to air. Sn⁴⁺/Sb/Bi based perovskite shows good stability but low performance. Efforts are being made to improve the performance by modification of morphology and crystallinity. Future seems to be very bright and promising of having Pb free perovskites which will have required optoelectronics performance along with a good stability and power conversion efficiency.

Suvankar Mondal et al. [7] studied and fabricated flexible, self-powered piezoelectric nanogenerator, which is sustainable, accessible and efficient energy alternative. CsPbBr₃ perovskite loaded into PVDF increases the electroactive β phase in PVDF more than 90%. It is quite worthy to be used as piezoelectric mechanical energy harvester. Energy generation from the devices also has been investigated through simple human movements like pressing by hand, finger touch, toe pressing, bending by arm etc. CsPbBr₃-PVDF composite based PNG showed

an output power of 4.24 mW, open-circuit voltage of 120 V and short-circuit current of 35 μ A. This flexible PNGs were able to light up several commercial LEDs. It showed how the output enhances due to the addition of filler perovskite material into PVDF. Output went maximum at 5% loading of CsPbBr₃. Photosensitivity of the composite films had been investigated under light, which also shows its potential use as photodetector. Synthesis of CsPbBr₃ and PVDF-CsPbBr₃ composite film preparation have been studied from this work.

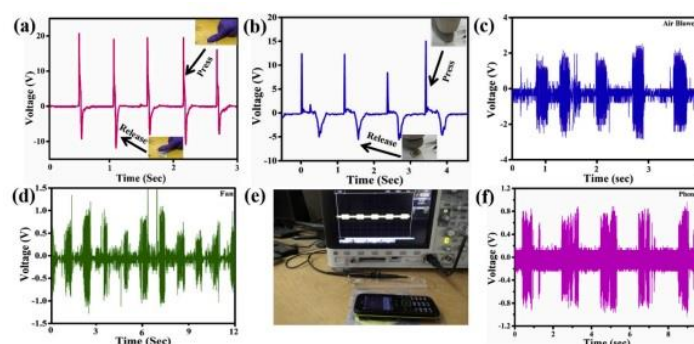


Fig. 2.1- Output voltage of PNG 5 (a) under the finger tapping (b) under toe pressing (c) due to air blower pressure (d) due to table fan air pressure (f) due to mobile vibration. (e) Digital image of the piezo-response under mobile vibration.

Richa Pandey et al. [8] reported a lead-free hybrid halide perovskite which has high piezoelectric charge density. They used Formamidinium Tin Iodide (FASnI₃) organic perovskite, in soft PVDF polymer matrix and resulted a high performance flexible piezoelectric nanogenerators. The device shows the output voltage of 23 V and power density of 35.05 mWcm⁻² across a 1M Ω resistor, under a periodic vertical compressive pressure, with a release pressure of 0.1 MPa. This study opens a path to examine organic-inorganic perovskite to be used as photodetectors, energy storage devices like capacitors and batteries (W. Zhang et al. [9]) etc. Ferroelectricity and piezoelectricity (W.-Q. Liao et al. [10]) exhibited by these materials have been interesting and these can be used in the field of mechanical energy harvesting application. Eco-friendly, highly efficient lead-free energy harvesting devices continue to fetch immense research activity headed towards further improving their present performance. Piezoelectric

nanogenerators (PENG) are such device which have the potential for applications because of their promising ability to generate electrical power locally through pressure, vibrations, movements using relatively simple device structures, low cost and large-scale production. This study has showed that the piezoelectric output energy achieved from the FASnI₃: PVDF composite nanogenerator is increased as compared to previously reported nanogenerators based on organic-inorganic hybrid metal halide perovskite materials. Incorporation of PVDF not only enhanced the ferroelectric properties of composite, but also provided an essential environmental and mechanical stability to FASnI₃. These nano-composite based devices are more compact and suitable to make flexible nanogenerator devices.

Cong Zhang et al. [11] focused their attention on the limitation of supply of fossil fuel, pollution, chemical batteries, and the many potential applications of wearable electronics, the development of more effective lightweight energy sources is important for future. Piezoelectric nanogenerators (PENGs) convert a mechanical energy into an electric energy and sometimes may even have the potential to replace conventional chemical batteries, many studies have evidences. This study shows how conventional textile has been replaced by PENG based smart textile. It has some special features like energy conversion and online health testing etc. Different electrode materials are also studied to improve output voltage. Baik et al. [12] increased the contact adhesion between PVDF and PPy using alkaline treatment and chemical vapor deposition. The group showed that PVDF-based nanogenerators with PPy electrodes, which produce a higher output voltage of 1.67 V than PVDF based nanogenerators with aluminum-foil electrodes. This paper also reviews the progress of research on textile-based PENGs, classification of piezoelectric materials, electrode materials, and tries to find ways to improve their piezoelectric performance. There are several methods of different device structures of textile-based PENGs are compared. Eventually, the most important concern for the application of textile-based PENGs are given to improve the future possibilities.

classification	categories	advantages	disadvantages
piezoelectric crystals	quartz crystal, ADP	high mechanical quality factor Q_m	The manufacturing process is difficult and expensive.
piezoelectric ceramics	BaTiO ₃ , K ₂ NaO ₃ , NaNbO ₃ , GaN, InN, CdS, ZnO, PbTiO ₃ , PbZrTiO ₃ , PZT, LiNbO ₃	high sensitivity, resistance to acids and bases, high coupling-factor and high dielectric constant	expensive to produce, brittle, low strain, heavy
piezoelectric polymers	PVDF, P(VDF-TrFE), P(VDF-HFP), PP, Nylon11, PAN	flexible, lightweight, low cost, lead free, easily processable	low energy-conversion rate and weak electromechanical coupling
piezoelectric composites	piezoelectric polymers + piezoelectric ceramics (e.g., PVDF + BaTiO ₃ , PVDF + PbTiO ₃)	synergistic effect	neutralization effect due to inconsistent polarization direction

Table 2.1- Different Piezoelectric materials, their merits and demerits

Bapi Pradhan et al. [13] reported all-inorganic perovskite nanocrystals are promising alternative of metal halide single perovskites. Cesium antimony halide (Cs₃Sb₂X₉, X = Cl, Br, I) perovskite nanocrystal materials are favorable for optoelectronic applications. They report on a colloidal synthesis of Cs₃Sb₂Cl₉ perovskite nanowires. They noted that there is a coexistence of trigonal and orthorhombic phases in the nanocrystals due to tuning the ratio of precursors, ligands and temperature variation. UV-vis absorption spectrum of NWs revealed an optical band gap of 3.4 eV. Whereas the reported band gap of bulk Cs₃Sb₂Cl₉ is ~3 eV. An increase in the band gap of the NWs attributed to the quantum confinement effect. Photoluminescence (PL) spectrum shows a peak maximum at 436 nm with quantum yield of 4%. Raman spectrum shows major peaks at 253 cm⁻¹ and 308 cm⁻¹. A good photo-responsive properties reveal prospects that these perovskite NCs materials for optoelectronic applications. This work also provides a procedure for the fabrication of environmentally friendly photodetectors.

A study of Chong Chen et al. [14] demonstrated that BiCl₃ influences the formation of β crystal of PVDF and enhancing the conductivity to good amount. It has drawn increasing attention in the fields of PVDF piezoelectric based energy harvesting (R. Guo et al. [15]) applications. The β -phase content was achieved from the film of PVDF doped with BiCl₃. It increases the piezoelectric energy output of the thin films. When subjected to vertical vibration, the output voltage of BiCl₃/PVDF composite film-based piezoelectric nanogenerator with a ratio of 2 wt% is up to 1.1V, which is 4.76 times higher than that of pure PVDF fiber. The peak current and

power density are $2 \mu\text{A}$ and $0.2 \mu\text{W}\cdot\text{cm}^{-2}$, respectively. The output signals generated from the BiCl₃/PVDF fiber film is used to charge a capacitor through a bridge rectifier and then light up a LED. Purpose of their study to provide the continuous power supply for these devices, which is an urgent problem to be taken care of. The rudimentary solution is to use chemical batteries. Due to its limited power, limited operating time, batteries would not be a good option for the future. Instead, the mechanical energy generated by the human body due to movement and converted into electrical energy these devices can give continuous power supply. The most feasible way to convert mechanical energy into electrical energy is to use piezoelectric nanogenerator (PENGs) based on piezoelectric materials. These have many advantages, such as small size, simple operation, simple construction, high sensitivity, durability and strength, flexibility and so on.

Composite nanofiber	Composite nanofiber PENG V_o	PVDF fiber PENG V_o	growth rate	Reference
graphene/PVDF	7.9 V	3.8 V	2.08	[37]
PVDF/MWCNTs	6 V	3 V	2.00	[38]
CNCs/PVDF	60 V	20 V	3.00	[39]
NiCl ₂ ·6H ₂ O/PVD F	0.762 V	0.296 V	2.57	[40]
BiCl ₃ /PVDF	1.0 V	0.21 V	4.76	Present work

Table 2.2- Output performance comparison of composite PENGs

Jun Yan et al. [16] demonstrated the perovskite metal halides have been drawing great attention because of their excellent photoelectric properties and structural simplicity. Here, the authors report a method for the controlled synthesis of cesium-bismuth halides by controlling the stoichiometric ratio of Cs/Bi precursors at room temperature. They have obtained 0D Cs₃BiCl₆ and 1D Cs₃Bi₂Cl₉ at the Cs/Bi feed ratio of 3:1 and 3:2, respectively. But both metal halides exhibit a very low photoluminescence quantum yield (PLQY) due to their intrinsic nature

of indirect band gaps. It is found that an appropriate amount of Mn^{2+} doping does not change the actual crystal structures of cesium-bismuth halides, but Mn 3d orbitals produce impurity states in the forbidden energy gaps of the pristine structure, which results in efficient energy transfer from the conduction band to d-state of Mn ions. These results show a range of possibility of low-dimensional metal halides and provide an important reference for the manipulation of crystal structure and optical properties of metal halide perovskite. $\text{Cs}_3\text{Bi}_2\text{Cl}_9$ metal halide doped Mn with adequate precursors give rise to the electrical conduction and optical properties. This study opens the door for metal halides to be used more efficiently as photodetectors.

S. Paul et al. [17] conducted a study on ligand free cesium antimony chloride ($\text{Cs}_3\text{Sb}_2\text{Cl}_9$) NCs synthesis process to overcome the drawbacks of using ligands. They have synthesized hexagonal shape NCs through a fast one step reaction at room temperature using a reprecipitation method. Then the shape of hexagonal NCs is further tuned into well-defined 2D plates by solid-state temperature-driven crystal phase transition, which resulted in irreversibility of trigonal to orthorhombic crystallographic phase transition. This study showed a coexistence of the major trigonal and minor orthorhombic phases. The ratio of trigonal to orthorhombic phases is expected to be the determining factor in the hexagonal-shaped NCs. The shape of the NCs was further tuned into well-defined ligand free 2D plates using temperature driven crystallographic phase transition. There are variety of perovskites (J. Pal et al. [18]) with the composition $\text{R}_3\text{M}_2\text{X}_9$ ($\text{R} = \text{Cs, K, Rb, etc.}$, and $\text{M} = \text{Fe, As, Bi, Sb, etc.}$, and $\text{X} = \text{Cl, I, Br}$) exist. Antimony containing perovskites have structural similarity with the hybrid organic inorganic lead halide perovskites, the trivalent Sb^{3+} contains a similar electronic configuration to the divalent Pb^{2+} , making it an alternative for Pb free perovskite. Even though ligand-free, both the hexagonal NCs and plates show ambient stability for over months. This method to design shape-controlled ligand-free perovskite NCs may find useful applications in optoelectronic devices in future.

Sidney E. Creutz et al. [19] reported Cesium bismuth halides (Cs-Bi-X) synthesis by a combination of hot-injection and post-synthetic anion exchange. These perovskites recently have been the subject of immense attention as possible less-toxic alternatives compared to lead halide perovskites. These can be used in luminescence and photovoltaics applications. Here, they prepared many structures and compositions, including several that have not been characterized before. They have also demonstrated different halide compositions, structural and optical properties of Cs_3BiX_6 ($\text{X} = \text{Cl}, \text{Br}, \text{I}$) nanocrystals and $\text{Cs}_3\text{Bi}_2\text{X}_9$ ($\text{X} = \text{Cl}, \text{Br}, \text{I}$) nanoplatelets. Spectroscopic characterizations ensure that those can be used in optoelectronic applications. This method gives isolation of hexagonal nanoplatelets $\sim 20\text{--}25$ nm in diameter and ~ 3 nm thick. The absorption spectra of the nanoplatelets are generally similar to those reported for bulk crystals and thin films (K. Bass et al. [20]). They anticipate that similar methods should allow to polycrystalline thin films also. This strategy can be powerful in the search for lead-free perovskite for optoelectronics applications.

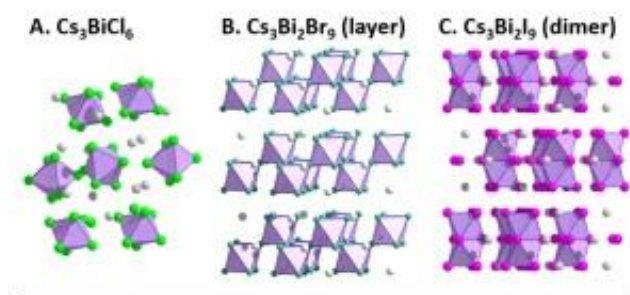


Fig. 2.2- Structures of Cs_3BiCl_6 , $\text{Cs}_3\text{Bi}_2\text{Br}_9$, and $\text{Cs}_3\text{Bi}_2\text{I}_9$ in Bulk

Abinash Pradhan et al. [21] conducted a study on bismuth substitution in $\text{Cs}_3\text{Sb}_2\text{Cl}_9$ and examined its phase transition. In this chapter, they have showed the structural stability of $\text{Cs}_3\text{Sb}_2\text{Cl}_9$ and the effect of Bi substitution on the structure and optical properties of the above phase. Pristine trigonal $\text{Cs}_3\text{Sb}_2\text{Cl}_9$ phase was obtained by reacting metal chlorides at $\leq 85^\circ\text{C}$, whereas pure orthorhombic phase was obtained at $\geq 130^\circ\text{C}$. Bi substitution in $\text{Cs}_3\text{Sb}_{2-x}\text{Bi}_x\text{Cl}_9$ gives mixture of trigonal and orthorhombic phases till $x < 0.1$ and further substitution ($x \geq 0.1$)

gives pure orthorhombic phase. Organic-inorganic hybrid and pure inorganic lead halide perovskites are of immense research interest because of the large-range of optoelectronic applications such as photodetectors, solar cells. But suffer from practical application in large scale because of the toxicity of lead as well as their poor stability towards light, heat, and atmospheric moisture.

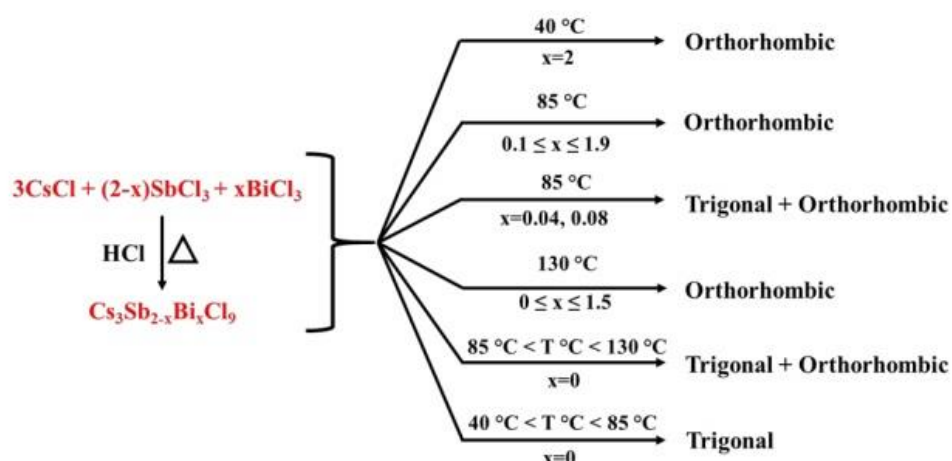


Fig. 2.3- Schematic diagram for the route of $\text{Cs}_3\text{Sb}_{2-x}\text{Bi}_x\text{Cl}_9$ series at different perovskite loaded composition and temperature.

Therefore, it is necessary to find alternatives of lead to be used as an element in perovskite. Bi, Sb are some promising alternatives which are less toxic, have excellent optoelectronic property and good environmental stability. Lead has been replaced by divalent cations like Sn^{2+} , Ge^{2+} trivalent cations like Sb^{3+} , Bi^{3+} (M. Leng et al. [22]) one monovalent and one trivalent cation¹⁴⁻¹⁶, tetravalent cations like Pd^{4+} and Sn^{4+} . It has been seen that the activation energy for the formation of orthorhombic phase in the solution is higher than the trigonal phase. They have done heat treatment on both orthorhombic and trigonal $\text{Cs}_3\text{Sb}_2\text{Cl}_9$ phases at 300°C . It confirms that trigonal phase is the thermodynamic stable phase while orthorhombic phase is metastable. Raman spectroscopic study confirms the phase transition with composition variation in $\text{Cs}_3\text{Sb}_{2-x}\text{Bi}_x\text{Cl}_9$. Single crystal study and Rietveld refinement shows that Bi prefers to occupy Sb crystallographic site.

References

- [1] Lu L, Ding W, Liu J, Yang B. Flexible PVDF based piezoelectric nanogenerators. *Nano Energy*. 2020 Dec 1;78:105251.
- [2] Wang R, Huang T, Xue J, Tong J, Zhu K, Yang Y. Prospects for metal halide perovskite-based tandem solar cells. *Nature Photonics*. 2021 Jun;15(6):411-25.
- [3] J. Hu and R. G. Gordon, *J. Appl. Phys.* 72 (1992) 5381
- [4] T. Minami, H. Nanto and S. Takata, *Jpn. J. Appl. Phys., Part 2: Lett.* 23 (1984) L280
- [5] W. O. Lytle and A. E. Junge, U.S. Patent No. 2,566,346, (1951)
- [6] R. Groth, *Phys. Status. Solidi* 14 (1966) 69
- [7] Mondal S, Paul T, Maiti S, Das BK, Chattopadhyay KK. Human motion interactive mechanical energy harvester based on all inorganic perovskite-PVDF. *Nano Energy*. 2020 Aug 1;74:104870.
- [9] J. L. Vossen, *RCA Rev.* 32 (1971) 269
- [10] S. J. Pearton, D. P. Norton, K. Ip, Y. W. Heo, and T. Steiner, *Prog. Mater. Sci.* 50, 293 (2005)
- [11] M. Snure and A. Tiwari, *J. Appl. Phys.* 101, 124912 (2007)
- [12] B. Kumar, H. Gong, and R. Akkipeddi, *J. Appl. Phys.* 98, 073703 (2005)
- [13] J. E. Medvedeva, *Phys. Rev. Lett.* 97, 086401 (2006)
- [14] Michael Snure, Ashutosh Tiwari, *App. Phys. Lett.* **91**, 092123 (2007)
- [15] (a) Hiroshi Yanagi, Shin-ichiro Inoue, Kazushige Ueda, Hiroshi Kawazoe, Hideo Hosono, and Noriaki Hamada, *Journal of Applied Physics* **88**, 4159 (2000); (b) H. Kawazoe, M. Yasukawa, H. Hyodo, M. Kurita, H. Yanagi, and H. Hosono, *Nature* **389**, 939 (1997) (c) K. Ueda, T. Hase, H. Yanagi, H. Kawazoe, H. Hosono, H. Ohta, M. Orita, and M. Hirano, *J. Appl. Phys.* **89**, 1790 (2001); (d) H. Yangi, T. Hase, S. Ibuki, K. Ueda, and H. Hosono, *Appl. Phys. Lett.* **78**, 1583 (2001)
- [16] Kazuhiko Tonooka, Katsuyoshi Shimokawa, Okio Nishimura, *Thin Solid Films* 411 (2002) 129–133
- [17] Carrie G. Read, Yiseul Park, and Kyoung-Shin Choi, *J. Phys. Chem. Lett.* 2012, 3, 1872–1876j
- [18] Pal J, Manna S, Mondal A, Das S, Adarsh KV, Nag A. Colloidal Synthesis and Photophysics of M₃Sb₂I₉ (M= Cs and Rb) Nanocrystals: Lead-Free Perovskites. *Angewandte Chemie*. 2017 Nov 6;129(45):14375-9.
- [19] Creutz SE, Liu H, Kaiser ME, Li X, Gamelin DR. Structural diversity in cesium bismuth halide nanocrystals. *Chemistry of Materials*. 2019 Jun 17;31(13):4685-97.
- [20] Sasaki S, Prewitt CT, Bass JD, Schulze WA. Orthorhombic perovskite CaTiO₃ and CdTiO₃: structure and space group. *Acta Crystallographica Section C: Crystal Structure*

Communications. 1987 Sep 15;43(9):1668-74.

[21] Pradhan A, Sahoo SC, Sahu AK, Samal SL. Effect of Bi substitution on Cs₃Sb₂Cl₉: structural phase transition and band gap engineering. *Crystal Growth & Design*. 2020 Apr 14;20(5):3386-95.

[22] Leng M, Bi J, Wang W, Liu R, Xia C. Synthesis and characterization of Ru doped NaNi_{0.5}Mn_{0.3}Ti_{0.2}O₂ cathode material with improved electrochemical performance for sodium-ion batteries. *Ionics*. 2019 Mar;25(3):1105-15.

Chapter -3

Instruments and apparatus

In this chapter major apparatus and accessories which were used while synthesis, are discussed along with the working principle and the operation of different characterization techniques has been given.

3.1 Crystal Structure Analysis

3.1.1. X-RAY Diffractometer

In the year 1895, the German physicist Roentgen discovered X-rays and so named due to the unknown nature at that time. These rays were invisible, traveled in straight lines and affected the photographic plate like ordinary light. Also, these rays show more penetrating power than light. In the year 1912, the exact nature of X-rays and diffraction phenomenon of x-rays by atomic planes of crystals were properly discovered. This discovery showed the wave nature of X-rays and explored a new direction to investigate the structure of matter. Solid matter can be divided as follows:

- **Amorphous:** The atoms are arranged in a random way similar to the disorder we find in a liquid. Glasses are amorphous materials.
- **Crystalline:** The atoms are arranged in a regular pattern, and one smallest volume element that by repetition in three dimensions describe the crystal. This smallest volume element is called a unit cell. The dimensions of the unit cell are described by three axes: a, b, c and the angles between them alpha (α), beta (β), gamma (γ). About 95% of all solids can be described as crystalline. X-rays are electromagnetic radiation of almost same nature as light but having

shorter wavelength of 0.5 to 2.5 Å regions. X-rays occupy the region between gamma and ultraviolet rays in the entire spectrum.

X-rays are electromagnetic radiation of almost same nature as light but having shorter wavelength of 0.5 to 2.5 Å regions. X-rays occupy the region between gamma and ultraviolet rays in the entire spectrum.

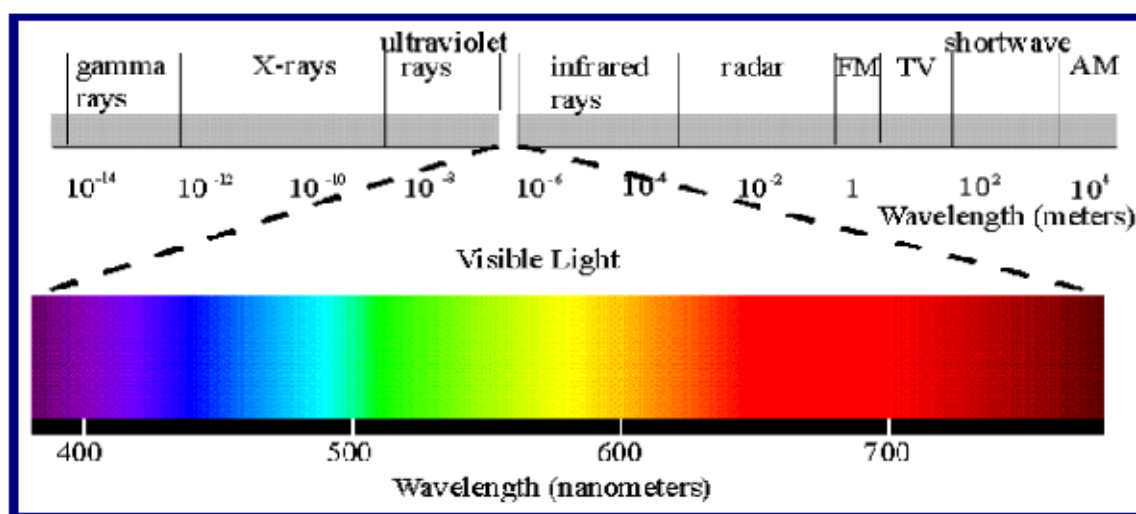


Fig 3.1: Illustration of electromagnetic spectrum

Diffraction is a scattering phenomenon in which a large number of atoms participate and act as scattering center. X-rays scattered by the atoms which are periodically arranged in the lattice, have definite phase relationship in between them. In some scattering direction, destructive interference takes place but in few directions, constructive interference occurs and forms the diffracted beam. *“A diffracted beam may be defined as a beam composed of a large number of scattered rays mutually reinforcing one another.”*

- **Working Principle**

In XRD, a collimated beam of X-rays is incident on a specimen and is diffracted by the crystalline phases in the specimen. Using Bragg equation for first order diffraction, lattice

spacing may be found from the diffraction angles. **Bragg's law** is the basic law which governs the X-ray diffraction technique of structural analysis. In **Bragg's law**, the interaction between x-rays and the electrons of the atoms is described as a process of reflection of x-rays by the atomic planes. When mono chromatic x-rays incident on the atoms in the crystal lattice, atomic planes allow a part of x-rays to pass through and reflect the other part, there exist a path difference in between the reflected rays from plane 1 and plane 2. These rays will reinforce each other, only when this path difference is equal to an integral multiple of the wavelength.

The **Bragg's law** can be written as:

$$2d\sin\theta = n\lambda$$

Where **n** is an integer and **λ** is the wavelength of the x-rays used, **θ** is Bragg's angle and **d** is the interplanar spacing.

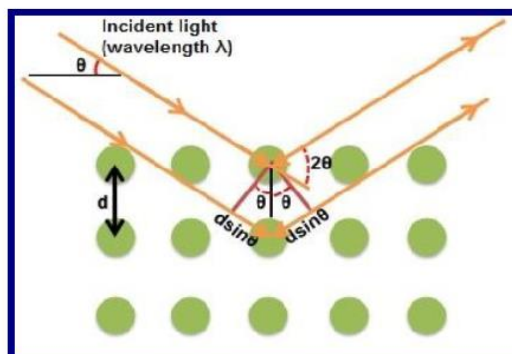


Fig 3.2: Illustration of Bragg's law
Diffractometer.

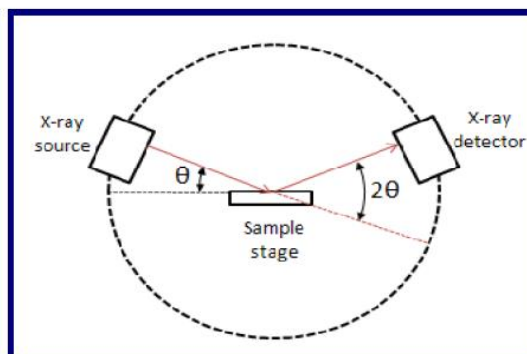


Fig 3.3: Schematic of X-ray.

- **Applications:**

- I.** Measurement of interplanar spacing between two atomic planes.
- II.** Determination of orientation of single crystal.
- III.** Determination of crystal structure for an unknown material.
- IV.** Measurement of particle size, phase and internal stress etc.

A RigakuUltima III X-ray diffractometer was used for recording the diffraction pattern of the samples in θ - 2θ configuration with Cu K α radiation ($\lambda = 1.5404 \text{ \AA}$) operated at 40 KV voltage and 30 mA current. A photographic image of X-ray diffractometer is shown in **Fig 3.4**.



Fig 3.4- Experimental set up of X-Ray Diffractometer.

3.2. Optical Property Analysis

3.2.1 Ultraviolet Visible Spectrophotometer

UV spectroscopy is type of absorption spectroscopy in which light of ultra violet region (200-400 nm) is absorbed by the molecule. Absorption of the ultraviolet radiations results in the excitation of the electrons from the ground state to higher energy state. The energy of the ultraviolet radiation that are absorbed is equal to the energy difference between the ground state and higher energy states ($\Delta E = h\nu$).

There are two laws that govern the absorption of light by a medium, known as **Lambert's law** and **Beer's law**. **Lambert's law** predicts that the absorbance is directly proportional to the thickness/path length of the medium. **Beer's law** explains the effect of concentration of colored components in solution on light transmission or absorption. By combining of these two laws, we get **Lambert- Beer's law** which is as follows:

$$\log (I_0/I_t) = A = \alpha cd$$

Where, A denotes absorbance, α denotes molar absorptivity, c is concentration and d is path length. From the **Lambert-Beer's law** it is clear that greater the number of molecules capable of absorbing light of a given wavelength, the greater the extent of light absorption. That is the basic principle of UV spectroscopy.

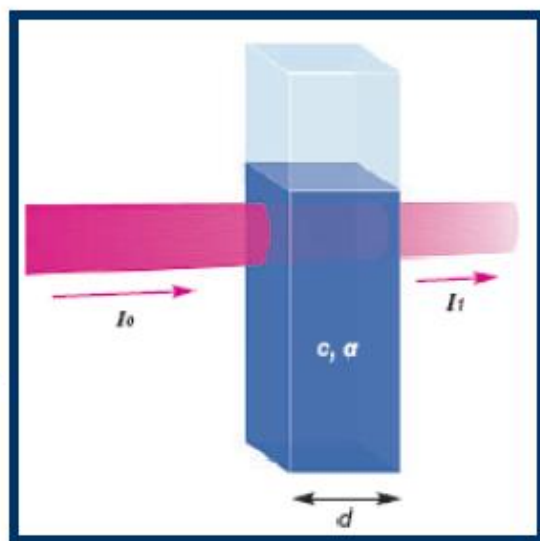


Fig 3.5- Illustration of Lambert-Beer's law

- **Configuration of instrument:**

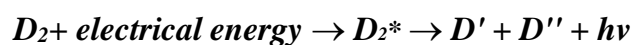
A spectrophotometer is an instrument which measures the transmittance or absorbance of a sample as a function of the wavelength of electromagnetic radiation. The main components of a spectrophotometer are:

1. Source
2. Monochromator
3. Sample container
4. Detectors

- **Source:**

The ideal light source would yield a constant intensity over all wavelengths with low noise and long-term stability. Unfortunately, however, such a source does not exist. Two sources are commonly used in UV-visible spectrophotometers. The electrical excitation of deuterium or hydrogen at low pressure produces a continuous UV spectrum. The mechanism for this

involves formation of an excited molecular species, which breaks up to give two atomic species and an ultraviolet-photon. This can be shown as;



Deuterium lamps emit radiation in the range 160-375 nm. Quartz windows must be used in these lamps, and quartz cuvettes must be used, because glass absorbs radiation of wavelengths less than 350 nm. The tungsten filament lamp is commonly employed as a source of visible light. This type of lamp is used in the wavelength range of 350-2500 nm.

- **Monochromator:**

All monochromators contain certain components like *entrance slit, collimating mirrors, dispersing device (usually a prism or a grating), focusing mirrors and exit slit*. Polychromatic radiation (radiation of more than one wavelength) enters the monochromator through the entrance slit. The beam is collimated, and then strikes the dispersing element at an angle. The beam is split into its component wavelengths by the grating or prism. By moving the dispersing element or the exit slit, radiation of only a particular wavelength leaves the monochromator through the exit slit.

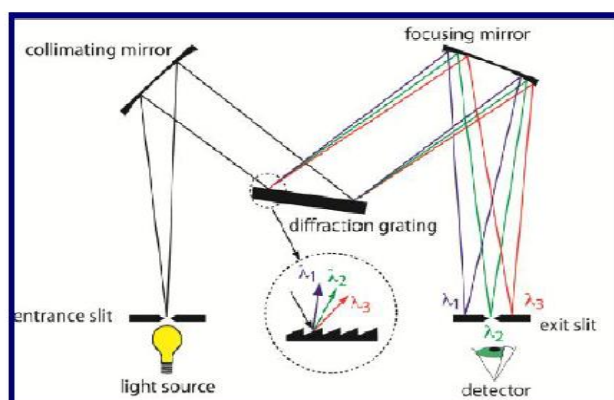


Fig 3.6- Construction of monochromator

- **Sample container:**

The containers (*cuvettes*) for the sample and reference solution must be transparent to the radiation which will pass through them. Quartz or fused silica cuvettes are required for spectroscopy in the UV region. These cells are also transparent in the visible region.

- **Detector:**

A detector converts a light signal into an electrical signal. The photomultiplier tube is commonly used detector in UV-Vis spectroscopy. It consists of *photoemissive cathode* (a cathode which emits electrons when struck by photons of radiation), several *dynodes* (which emit several electrons for each electron striking them) and an *anode*. Another type of detector is linear photodiode array which is an example of a *multichannel photon detector*. These detectors are capable of measuring all elements of a beam of dispersed radiation simultaneously. Photodiode arrays are complex devices but, because they are solid state, have high reliability.



Fig 3.8- Experimental set up of UV-Visible spectrophotometer.

3.3 Morphological analysis:

3.3.1 Field Emission Scanning Electron Microscope (FESEM):

The word *microscope* is derived from the Greek *mikros*(small) and *skopeo*(look at). From the discovery of science there has been an interest in being able to look at smaller and smaller details of the world around us. Our human eye provides the extreme limitation in microscopy. It has a resolution power of ~ 0.1 mm, which is equivalent to the diameter of a human hair. This means that two small objects placed about 20 cm from the eye can be viewed as distinct when they are ~ 0.1 mm apart. The limitation arises from the intrinsic magnification power of human eye and the separation of the sensing elements on the retina. An optical microscope has a resolution power and improvement of power than that of the unaided eye can be done in a way which is limited by the wavelength of the light used to illuminate the object. For visible light, this corresponds to power ~ 0.2 μm . That's why below 0.2 μm , we can not visualize objects through optical microscope. A FESEM is an electron microscope which uses electron beam liberated by field emission source instead of light.

Electrons will not travel far through air and electron microscopes are usually vacuum based instruments. Image formation in the SEM depends on the signals produced from the electron beam and specimen interactions. These interactions can be classified into two major categories: *elastic interactions* and *inelastic interactions*. Elastic scattering results from the deflection of the incident electron by the atomic nucleus or outer shell electrons of the specimen. This kind of interaction is characterized by very small amount of energy loss during the collision and by a wide angle directional change of the scattered electron. Incident electrons that are elastically scattered through an angle of more than 90° are called *backscattered electrons (BSE)*, and produce a useful signal for imaging the sample. Inelastic scattering occurs through a variety

of interactions between the incident electrons and the electrons and atoms of the sample and results in the primary beam electron transferring considerable amount of energy to that atom. The amount of energy loss depends on whether the specimen electrons are excited singly or collectively and on the binding energy of the electron to the atom. The most widely used signal produced by the interaction of the primary electron beam with the specimen is the *secondary electron emission* signal. When the primary beam strikes the sample surface causing the ionization of specimen atoms, loosely bound electrons may be emitted and these are referred to as secondary electrons. As they have low energy, typically an average of around 3–5 eV, they can only escape from a region within a few nanometers of the material surface. These can be used to give information about the surface topography, morphology of the sample with good resolution. In addition to these signals, a number of other signals are produced when an electron beam strikes a sample, including the emission of *continuous x-rays*, *characteristic x-rays*, *Auger electrons* and *cathodoluminescence*.

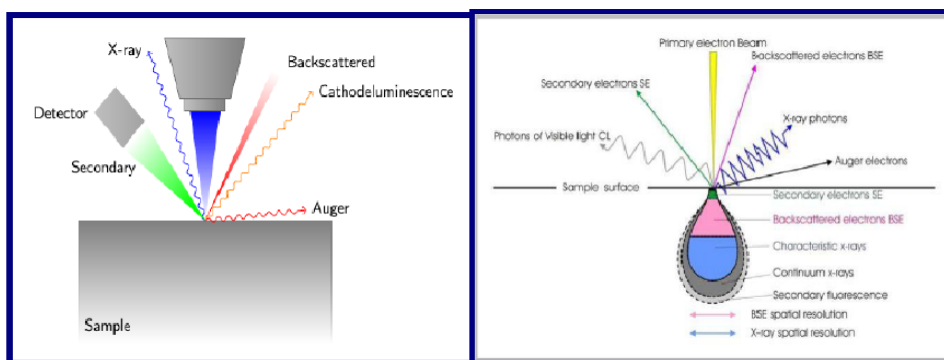


Fig 3.9- Interaction of electron beam with matter.

- **Configuration of FESEM:**

Fig 3.9 shows the total components of Field emission scanning electron microscope in details. It consists of electron gun to generate electron beam, electromagnetic lenses and aperture to focus the electron beam, detector, and vacuum system.

- **Electron Gun:**

The electron gun produces a stable electron beam with high current, small spot size, adjustable energy and small energy dispersion. The first generation SEM system generally used thermionic emission sources like tungsten “hairpin” ($\Phi=4.5\text{eV}$) or lanthanum hexaboride (LaB_6) ($\Phi=2.4\text{eV}$) cathodes, but for the modern FESEMs, the trend is to use field emission sources, which provide enhanced current and lower energy dispersion. Emitter lifetime is another important issue for selection of electron sources. The most widely used electron gun is composed of three parts: a Vshaped hairpin tungsten filament (the cathode), a Wehnelt cylinder and an anode, as shown in figure.

Thermionic sources require a high temperature to overcome the work function of the metal so that the electrons can escape from the cathode. Though they are inexpensive and the requirement of vacuum is relatively low but there are certain disadvantages, such as short lifetime, low brightness, and large energy spread which restrict their applications. For modern electron microscopes, field emission electron guns (FEG) are a good alternative for thermionic electron guns. In the FEG, a single crystal tungsten wire with very sharp tip is used as the electron source. In this system, a strong electric field forms on the finely oriented tip and the electrons are drawn toward the anodes forms concentrated electron beam.

- **Electron Lenses:**

Electron beam can be focused by electrostatic or magnetic field. But electron beam controlled by magnetic field has smaller aberration, so only magnetic field is employed in SEM system. Coils of wire, known as “electromagnets” are used to produce magnetic field and the trajectories of the electrons can be adjusted by the current applied on these coils.

- **Condenser lens:**

The electron beam will diverge after passing through the anode plate from the emission source. By using the condenser lens, the electron beam is converged and collimated into a relatively parallel stream. A magnetic lens generally consists of two rotationally symmetric iron pole

pieces in which there is a copper winding which provides magnetic field. There is a hole in the center of pole pieces that allows the electron beam to pass through. A lens-gap separates the two pole pieces, at which the magnetic field focuses the electron beam. The position of the focal point can be controlled by adjusting the condenser lens current.

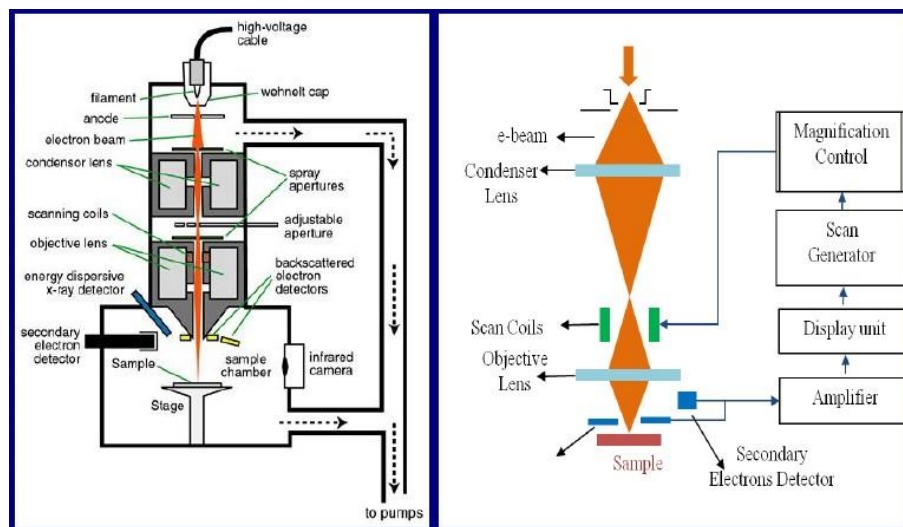


Fig 3.10- Configuration of FESEM and its different components

- **Scan Coils:**

The scan coils deflect the electron beam over the object according to a zigzag pattern. The formation of the image on the monitor occurs in synchrony with this scan movement. The scan velocity determines the refreshing rate on the screen and the amount of noise in the image. Scan coils often consist of upper and lower coils, which prevent the formation of a circular shadow at low magnification.

- **Objective lens:**

The objective or "probeforming" lens is located at the base of electron column just above sample. The beam is again divergent after passing through the apertures below the condenser

lens and must be convergent again. The objective lens focuses the electron beam onto the sample and controls final size and position.

- **Sample preparation:**

As we mentioned earlier that FESEM is vacuum based instrument, so sample must be vacuum tolerant. In addition to that, strong radiation by electrons can damage or destroy a sample through heating or other effects. Even in quite good vacuum (10^{-8} mbar), samples can become coated with gold/platinum in the microscope to retain the true surface details. Some samples, those are insulating in nature, are charged up under the electron beam and repel the incoming electron beam. This degrades the resolution and usually requires some prevention technique such as coating the sample with a conducting layer.

3.3.2 Energy dispersive X-ray analysis (EDAX)

This technique gives an overall mapping of the sample by analyzing near-surface elements and estimates the elemental proportion in percentages at different positions.

EDX is used in conjugation with SEM. An electron beam with energy of 10–20 keV strikes the conducting sample's surface, causing X-rays to emit from the material, and the energy of the emitted X-rays depend on the material under examination.

EDX does not fit under a technique for surface science, as the X-rays are generated in a region of about 2 microns in depth. By moving the electron beam across the material, an image of each element in the sample can be obtained. It generally takes long hours to acquire the images, as the intensity of the X-ray is low.

The composition or amount of nanoparticles near and at the surface can be estimated using the EDX, provided they contain some heavy metal ions. For instance, nanoparticles like silver, gold, and on the surface can be easily identified using EDX.



Fig 3.11: FESEM (Hitachi S-4800) set up.

3.4 Analysis of absorbance spectra and molecular vibrations:

3.4.1 Fourier transform infrared spectroscopy (FTIR):

FTIR Spectroscopy, fourier-transform infrared spectroscopy, is concerned with the vibration of molecules. Each functional group has its own discrete vibrational energy which can be used to identify a molecule through the combination of all of the functional groups. This makes FTIR microscopy ideal for sample ID, multilayer film characterization, and particle analysis. The electromagnetic spectrum consists of different regions corresponding to different energy (E), frequency (ν), and wavelength (λ) ranges as seen in Figure 1. The unit for near-, mid-, and far-infrared, the wavenumber (cm^{-1}), is derived from the inverse relationship between wavelength and frequency.

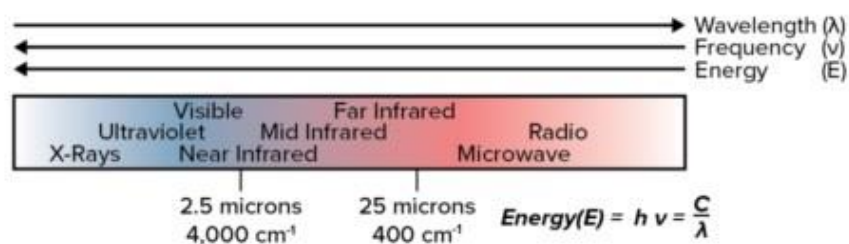


Fig. 3.12- Electromagnetic spectrum showing near and far infrared regions.

FTIR spectroscopy takes advantage of how IR light changes the dipole moments in molecules that correspond to a specific vibrational energy. Vibrational energy corresponds to two variables: reduced mass (μ) and bond spring constant (k). For k constant, we can look at C-C, C=C, and C≡C showing an increase of 800 cm^{-1} across the series. Substituting atoms in a C-C bond with nitrogen and oxygen causes a shift of 100 cm^{-1} . By looking at the two series, it can be seen that bond strength alters the wavenumbers more than mass.

Since every functional group is composed of different atoms and bond strengths, vibrations are unique to functional groups, and classes of functional groups (e.g. O-H and C-H stretches appear around 3200 cm^{-1} and 2900 cm^{-1} , respectively). A correlation chart with various functional group vibrations can be seen. Since the collection of vibrational energy bands for all of the functional groups a molecule is unique to every molecule, these peaks can be used for identification using library searches of comprehensive sample databases.

Working principle and different parts of FTIR

The three major parts of an FTIR are the source, interferometer, and detector. The source is typically a broadband emitter such as a mid-IR ceramic source ($50\text{--}7,800\text{ cm}^{-1}$), a near-IR halogen lamp ($2,200\text{ -- }25,000\text{ cm}^{-1}$), or a far-IR mercury lamp ($10\text{--}700\text{ cm}^{-1}$). The interferometer is the heart of FTIR and consists of a beam-splitter, a stationary mirror, a moving mirror, and a timing laser (box in figure 4). The beam-splitter splits the light from a source into two paths with half the light going to a stationary mirror and the other half going to a moving

mirror. In many FTIR systems, the beam-splitter is placed at 45 degrees to the incident beam, but for high throughput applications, a low angle interferometer is preferred as the P and S polarizations converge close to the Brewster's Angle. Common beam-splitter materials are KBr ($375 - 12,000 \text{ cm}^{-1}$) for mid-IR, Quartz ($4,000 - 25,000 \text{ cm}^{-1}$) for near-IR, and Mylar ($30 - 680 \text{ cm}^{-1}$) for far-IR. The beams from the moving and stationary mirrors are recombined back at the beam-splitter and steered toward the sample. The difference in the path of the mirrors causes constructive and destructive interference over the course of time it takes for the moving mirror to make a pass. The signal versus mirror position (and, thus, time) is called an interferogram. A laser is used to determine the position of the moving mirror using the precisely known wavelength of the laser (Figure 5). He-Ne lasers are the industry norm due to their excellent wavelength stability compared to solid-state or diode lasers. This laser stability allows for spectral additions, library searches, and other functions that need high wavenumber accuracy.

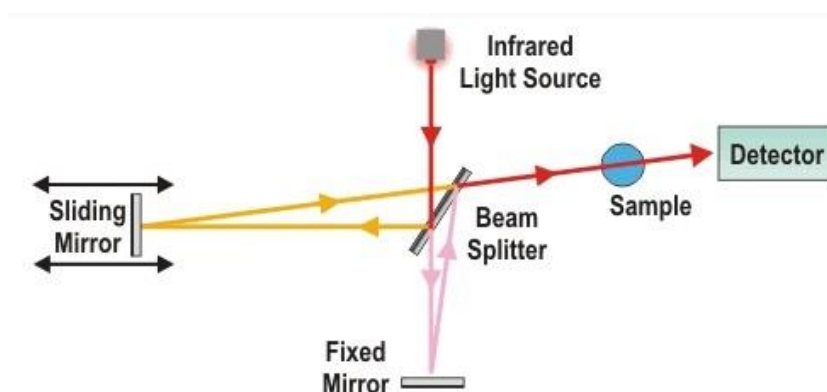


Fig. 3.13- Different parts and working of FTIR spectroscopy

- **Near infrared**

The Near-IR portion of the electromagnetic spectrum falls between $4,000$ to $12,800 \text{ cm}^{-1}$. This region consists of overtones (two of the same vibrational modes occurring simultaneously) and combinations (two different vibrational modes occurring simultaneously). Since these modes are not strictly quantum mechanically allowed, the intensity of the modes is often quite low.

These spectra are often complex, and chemometric techniques, such as multivariate analysis, are used. In spite of the drawbacks, there are clear advantages to Near-IR spectroscopy. Firstly, the path length of the light is such that bulk samples can be analyzed with little to no sample preparation. Secondly, water does not affect signal as it does in mid-IR.

- **Far infrared**

The Far Infrared region lies between 10 cm^{-1} and 700 cm^{-1} . The bonds that show in this region are 3+ atom functional groups, such as -C-C-C- bending, and lattice vibrations in crystalline materials. Since these are highly dependent on conformation or crystal structure, materials with the same chemical structure, but different crystal structures may be distinguished using Far-IR.



Fig. 3.14- FTIR spectroscopy machine

3.5 Electrical quantity analysis:

3.5.1 Measurement by cathode ray oscilloscope (CRO):

The cathode ray oscilloscope is an electronic test instrument, it is used to obtain waveforms when the different input signals are given. In the early days, it is called as an Oscillograph. The oscilloscope observes the changes in the electrical signals over time, thus the voltage and time describe a shape and it is continuously graphed beside a scale. By seeing the waveform, we can analyze some properties like amplitude, frequency, rise time, distortion, time interval, and etc.

Different parts and working principle of CRO

The CRO working principle depends on the electron ray movement because of the electrostatic force. Once an electron ray hits a phosphor face, then it makes a bright spot on it. A Cathode Ray Oscilloscope applies the electrostatic energy on the electron ray from two vertical ways. The spot on the phosphor monitor turns due to the effect of these two electrostatic forces which are mutually perpendicular. It moves to make the necessary waveform of the input signal.

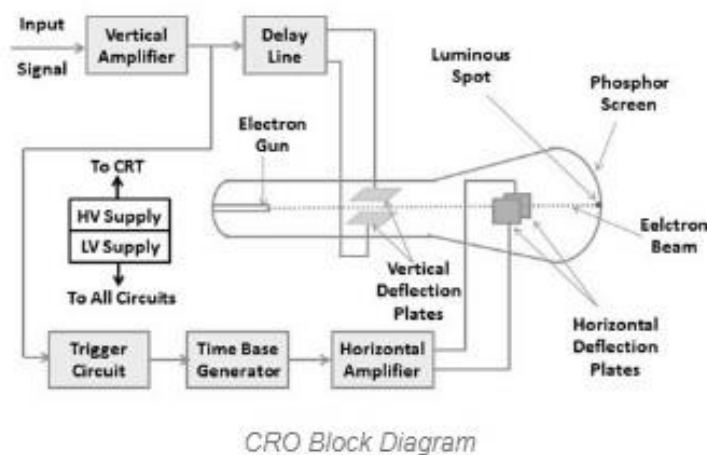


Fig. 3.15- Block diagram of CRO

Cathode Ray Tube

The CRO is the vacuum tube and the main function of this device is to change the signal from electrical to visual. This tube includes the electron gun as well as the electrostatic deflection plates. The main function of this electron gun is used to generate a focused electronic ray that speeds up to high frequency. The vertical deflection plate will turn the ray up & down whereas

the horizontal ray moved the electrons beams from the left side to the right side. These actions are autonomous from each other and thus the ray may be located anyplace on the monitor.

Electronic Gun Assembly

The main function of the electron gun is to emit the electrons to form them into a ray. This gun mainly includes a heater, a grid, cathode, and anodes like accelerating, pre-accelerating & focusing. At the cathode end, the strontium & barium layers are deposited to obtain the high electrons emission of electrons at the moderate temperature, the layers of barium, and are deposited at the end of the cathode. Once the electrons are generated from the cathode grid, then it flows throughout the control grid that is generally a nickel cylinder through a centrally situated co-axial by the axis of CRT. So, it controls the strength of the generated electrons from the cathode. When electrons flow throughout the control grid then it accelerates with the help of a high positive potential which is applied to the pre-accelerating or accelerating nodes. The electron ray is concentrated on electrodes to flow throughout the deflection plates like horizontal and vertical & supplies on to the fluorescent lamp.

Accelerating anodes

The anodes like accelerating & pre-accelerating are connected to 1500v & the focusing electrode can be connected to 500v. The electron ray can be focused on using two techniques like Electrostatic & Electromagnetic focusing. Here, a cathode ray oscilloscope utilizes an electrostatic focusing tube.

Deflecting Plate

Once the electron ray leaves the electron gun then this ray will pass throughout the two sets of the deflecting plate. This set will generate the vertical deflection that is known as Y plate's otherwise vertical deflecting plate. The set of the plate is used for a horizontal deflection which is known as X plate's otherwise horizontal deflection.

Fluorescent Screen of CRT

In the CRT, the front face is known as the faceplate, For the CRT screen, it is flat and its size is about 100mm×100mm. The CRT screen is somewhat bent for bigger displays and the formation of faceplate can be done by pressing the molten glass into a form & after that heating it. The inner face of the faceplate is covered by using phosphor crystal to change the energy from electrical to light. Once an electronics ray hits phosphor crystal, the energy level can be enhanced & thus light is generated throughout phosphorous crystallization, so this occurrence is known as fluorescence.

Glass Envelope

It is an extremely evacuated conical form of construction. The inside faces of the CRT among the neck as well as the display are covered through the aquadag. This is a conducting material that acts like a high-voltage electrode. The surface of the coating is connected electrically toward the accelerating anode to help the electron to be the center.

Vertical Deflection System

The main function of this amplifier is to amplify the weak signal so that the amplified signal can produce the desired signal. To examine the input signals are penetrated to the vertical deflection plates through the input attenuator and the number of amplifier stages.

Horizontal Deflection System

The vertical and horizontal system consists of horizontal amplifiers to amplify the weak input signals, but it is different from the vertical deflection system. The horizontal deflection plates are penetrated by a sweep voltage that gives a time base. By seeing the circuit diagram the sawtooth sweep generator is triggered by the synchronizing amplifier while the sweep selector switches in the internal position. So the trigger saw tooth generator gives the input to the horizontal amplifier by following the mechanism. Here we will discuss the four types of sweeps.

Recurrent Sweep

As the name, itself says that the sawtooth is respective that is a new sweep is started immodestly at the end of the previous sweep.

Triggered Sweep

Sometimes the waveform should be observed that it may not be predicted thus, the desired that the sweep circuit remains inoperative and the sweep should be initiated by the waveform under the examination. In these cases, we will use the triggered sweep.

Driven Sweep

In general, the drive sweep is used when the sweep is free-running but it is triggered by the signal under the test.

Non-Saw Tooth Sweep

This sweep is used to find the difference between the two voltages. By using the non-sawtooth sweep. We can compare the frequency of the input voltages.

Synchronization

The synchronization is done to produce a stationary pattern. The synchronization is between the sweep and the signal should measure. There are some sources of synchronization that can be selected by the synchronization selector. Which are discussed below.

Internal

In this, the signal is measured by the vertical amplifier and the trigger is abstained by the signal.

External

In the external trigger, the external trigger should be present.

Line

The line trigger is produced by the power supply.

Intensity Modulation

This modulation is produced by inserting the signal between the ground and cathode.

This modulation causes by brightening the display.

Positioning Control

By applying the small independent internal direct voltage source to the detecting plates through the potentiometer the position can be controlled and also we can control the position of the signal.

Intensity Control

The intensity has a difference by changing the grid potential with respect to the cathode.

Electrical Quantities Measurements

Electrical quantities measurements by using CRO can be done like amplitude, time period and frequency.

- Measurement of Amplitude
- Measurement of Time Period
- Measurement of Frequency
- Measurement of amplitude

The displays like CRO is used to exhibit the voltage signal like a time function on its display. The amplitude of this signal is stable; however, we can change the number of partitions that cover up the voltage signal within vertical way by changing volt/division button on top of the CRO board. So, we will acquire the signal's amplitude, which is there on the CRO screen with the help of the below formula.

$A = j * nv$; Where, 'A' is the amplitude, 'j' is the volt/division value, 'nv' is the no. of partitions that cover up the signal within a vertical way.

Measurement of Time Period

CRO displays the voltage signal as a function of time on its screen. The Time period of that periodic voltage signal is constant, but we can vary the number of divisions that cover one complete cycle of the voltage signal in the horizontal direction by varying the time/division knob on the CRO panel.

Therefore, we will get the Time period of the signal, which is present on the screen of CRO by using the following formula.

$$T = k * nh$$

Where, 'T' is the Time period, 'j' is the time/division value, 'nv' is the number of partitions that cover up one whole cycle of the periodic signal within the horizontal way.

Measurement of Frequency

On the CRO screen, the measurement of tile & frequency can be done very simply through the horizontal scale. If you want to make sure accuracy while measuring a frequency, then it assists to enhance the area of the signal on your CRO display so that we can more simply convert the waveform.

Initially, the time can be measured with the help of the horizontal scale on the CRO & counting the number of flat partitions from one finish of the signal to the other wherever it crosses the flat line. After that, we can develop the number of flat partitions through the time or division to discover the time period of the signal. Mathematically the measurement of the frequency can be signified as frequency = 1/period. $f = 1/T$



Fig.- 3.16 Keysight EDUX 1002A Cathode ray oscilloscope

3.6 Surface characterization analysis:

3.6.1 X-ray photo electron spectroscopy:

X-Ray Photoelectron Spectroscopy is one of the most powerful surface analytical techniques capable to provide accurate qualitative elemental analysis (for all elements except hydrogen and helium), quantitative composition and determination of chemical state such as binding and oxidation can also be done. The information should be originated within ~10 nm from the outer surface.

- **Basic principles of XPS:**

XPS is based on the photoelectric effect which is discovered by Hertz in 1887. In this case, electron emission from the surface is resulted due to the interaction of an x-ray photon of sufficient energy with the solid surface. The applied x-ray of 1-15 KeV energy is capable to induce electrons not only from the outer shells but also from the core levels of all elements of

$$h\nu = E_b + E_{kin} + W_f$$

periodic table. The governing equation of this phenomenon is as follows:

Where, E_b is binding energy, E_{kin} is kinetic energy of photoelectron, W_f is work function of the instrument.

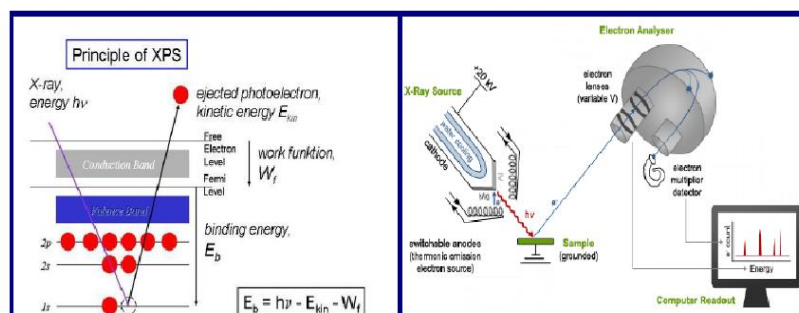


Fig 3.16- Basic principles and constructions of XPS.

- **Configuration of XPS instrument:**

The experimental set up contains mainly the following parts: (i) an X-ray source for XPS, (ii) an electron energy analyzer, combined with a detection system and (iii) a sample stage, all contained within a vacuum chamber. As for most techniques, the system is operated and controlled by a computer, usually provided with software allowing mathematical treatment.

- **X-ray source:**

Since XPS is concerned with the analysis of core electrons from a solid surface, sources used in XPS must be able to produce photons of a sufficient energy to access a suitable number of core electron levels. Photons of this energy lie within the X-ray region of the electromagnetic spectrum. As a result, these are otherwise referred to as X-rays. X-ray tubes produce X-rays by directing a sufficiently energetic electron beam at some metallic solid. This metallic object is referred to as the X-ray anode, with the electron source being the cathode. Although any solid can in principle be used as an X-ray anode, Al has become that most commonly used in XPS due to the relatively high energy and intensity of Al- $K\alpha$ X-rays, the minimal energy spread of Al- $K\alpha$ X-rays and the fact that Al is an effective heat conductor.

- **Electron energy analyzer:**

Since information in XPS is derived from the E_{kin} of the electron emissions, effective analysis requires energy filter that exhibits both a high-energy resolution and a high transmission. The former allows for the separation of closely spaced peaks, thereby optimizing speciation identification capabilities, while the latter allows for sensitivity to be maximized. The two primary energy filter configurations used in XPS named *Cylindrical Mirror Analyzer (CMA)*, *Concentric Hemispherical Analyzer (CHA)*.

- **Detector:**

In XPS, it is not only important to measure the energy of the electron emissions but also the number of electrons produced. XPS spectra is plotted in units of energy versus intensity, with the energy defined by the energy analyzer used and the intensity defined by the number of electrons recorded by the detector. To obtain the best possible sensitivity, the detector must be capable of recording individual electrons, that is, operating in pulse counting mode. This signal is recorded in units of current (A), which are then represented in units of counts per second.

- **Sample stage:**

The mounting of the samples on the sample holder should be done in such a way that electrical conduction is guaranteed. This is achieved by using metallic clips or bolt-down assemblies. Alternatively, a metal loaded tape may also be used. In the case of powders, the particles can be pressed into an indium foil or carbon tape.

- **Vacuum requirement:**

As XPS is a surface sensitive method, impurities can play a major role in the observed spectra. The criterion is that a good vacuum is needed to maintain the integrity of the surface. In general, 10^{-5} Torr is sufficient to allow the photoelectron to reach the detector without suffering collisions with other gas molecules. On the other hand, 10^{-9} Torr or lower is required to keep an active surface clean for more than several minutes. So, 10^{-8} - 10^{-9} Torr provides a reasonable pressure range for XPS measurement. Sample analysis was performed on the SPECS with hemispherical energy analyzer (HAS 3500). Photoelectrons were excited using the monochromatic Mg K α X-ray (1253.6 eV) or Al K α X-ray (1486.6 eV) was used as the excitation source operated at 10 kV and with an anode current 17 mA. The photograph of the X-ray photoelectron spectroscopy is shown in the **Fig 3.17**



Fig 3.17- Experimental set up of XPS.

3.7 Measurement of dielectric property by impedance analyzer:

3.7.1 Measurement of dielectric constant and dielectric loss:

The material properties that would be discussed here are permittivity and permeability. Resistivity is another material property which will not be discussed here. Information about resistivity and its measurement can be found in the Solutions for measuring Permittivity and Permeability with LCR Meters and Impedance Analyzers application note. It is important to note that permittivity and permeability are not constant. They can change with frequency, temperature, orientation, mixture, pressure, and molecular structure of the material.

Dielectric constant A material is classified as “dielectric” if it has the ability to store energy when an external electric field is applied. If a DC voltage source is placed across a parallel plate capacitor, more charge is stored when a dielectric material is between the plates than if no material (a vacuum) is between the plates. The dielectric material increases the storage capacity of the capacitor by neutralizing charges at the electrodes, which ordinarily would contribute to the external field. The capacitance with the dielectric material is related to dielectric constant. If a DC voltage source V is placed across a parallel plate capacitor (Figure

3.18), more charge is stored when a dielectric material is between the plates than if no material (a vacuum) is between the plates.

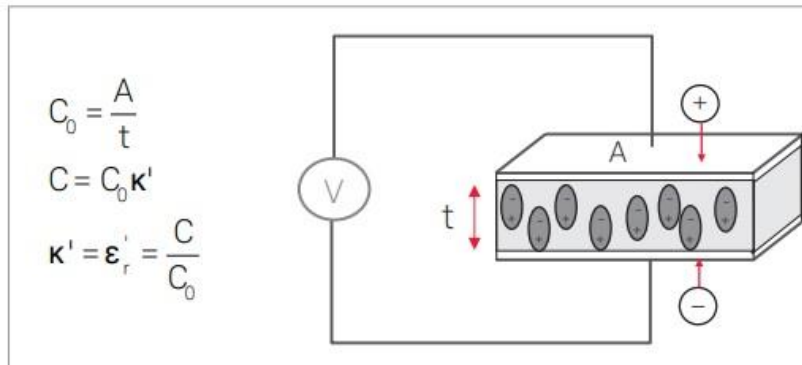


Fig. 3.18- A parallel plate capacitor under DC source

Where C and C_0 are capacitance with and without dielectric, $\kappa' = \epsilon_r'$ is the real dielectric constant or permittivity, and A and t are the area of the capacitor plates and the distance between them (Figure 1). The dielectric material increases the storage capacity of the capacitor by neutralizing charges at the electrodes, which ordinarily would contribute to the external field. The capacitance of the dielectric material is related to the dielectric constant as indicated in the above equations. If an AC sinusoidal voltage source V is placed across the same capacitor (Figure 2), the resulting current will be made up of a charging current I_c and a loss current I_l that is related to the dielectric constant. The losses in the material can be represented as a conductance (G) in parallel with a capacitor (C).

The complex dielectric constant k consists of a real part κ' which represents the storage and an imaginary part κ'' which represents the loss. The following notations are used for the complex dielectric constant interchangeably $\kappa = \kappa^* = \epsilon_r = \epsilon_r^*$. From the point of view of electromagnetic theory, the definition of electric displacement (electric flux density) D_f is:

$$D_f = \epsilon E$$

where $\epsilon = \epsilon^* = \epsilon_0 \epsilon_r$ is the absolute permittivity (or permittivity), ϵ_r is the relative permittivity.

$\epsilon_0 \approx (1/36 \pi) \cdot 10^{-9}$ F/m is the free space permittivity and E is the electric field. Permittivity describes the interaction of a material with an electric field E and is a complex quantity.

$$k = \epsilon / \epsilon_0 = \epsilon_r - j\epsilon_r''$$

Dielectric constant (k) is equivalent to relative permittivity (ϵ_r) or the absolute permittivity (ϵ) relative to the permittivity of free space (ϵ_0). The real part of permittivity (ϵ_r) is a measure of how much energy from an external electric field is stored in a material. The imaginary part of permittivity (ϵ_r'') is called the loss factor and is a measure of how dissipative or lossy a material is to an external electric field. The imaginary part of permittivity (ϵ_r'') is always greater than zero and is usually much smaller than (ϵ_r). The loss factor includes the effects of both dielectric loss and conductivity.

When complex permittivity is drawn as a simple vector diagram (Figure 3.19), the real and imaginary components are 90° out of phase. The vector sum forms an angle δ with the real axis (ϵ_r'). The relative “lossiness” of a material is the ratio of the energy lost to the energy stored.

$$\tan \delta = \epsilon_r'' / \epsilon_r' = \text{Energy lost per cycle} / \text{Energy stored per}$$

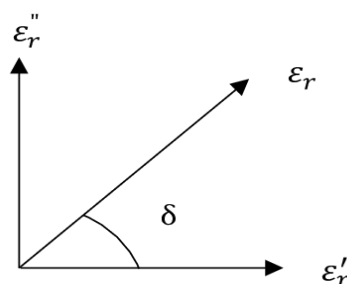


Fig. 3.19- Loss tangent $\tan \delta$ for a lossy capacitor

Measuring system

Network analyzers

A measurement of the reflection from and/or transmission through a material along with knowledge of its physical dimensions provides the information to characterize the permittivity and permeability of the material. Vector network analyzers such as the PNA family, ENA series and Field Fox make swept high frequency stimulus-response measurements from 9 kHz to 1.1 THz. A vector network analyzer consists of a signal source, a receiver and a display. The source launches a signal at a single frequency to the material under test. The receiver is tuned to that frequency to detect the reflected and transmitted signals from the material. The measured response produces the magnitude and phase data at that frequency. The source is then stepped to the next frequency and the measurement is repeated to display the reflection and transmission measurement response as a function of frequency. More information on the network analyzer functioning and architecture is in Solutions for Measuring Permittivity and Permeability with LCR meters and Impedance analyzers and understanding the Fundamental Principles of Vector Network Analysis application notes. Simple components and connecting wires that perform well at low frequencies behave differently at high frequencies. At microwave frequencies wavelengths become small compared to the physical dimensions of the devices such that two closely spaced points can have a significant phase difference. Low frequency lumped-circuit element techniques must be replaced by transmission line theory to analyze the behavior of devices at higher frequencies. Additional high frequency effects such as radiation loss, dielectric loss and capacitive coupling make microwave circuits more complex and expensive. It is time consuming and costly to try to design a perfect microwave network analyzer.

Impedance analyzers and LCR meters

Impedance analyzers and LCR meters such as the ones listed in Figure 12 are used to measure the material properties at lower frequencies. The material is stimulated with an AC source and the actual voltage across the material is monitored. Material test parameters are derived by knowing the dimensions of the material and by measuring its capacitance and dissipation factor.



Fig. 3.20- Agilent 4294A Impedance analyzer, LCR meter

Chapter -4

Colloidal synthesis and characterization of $\text{Cs}_3\text{SbBiCl}_9$ perovskite

4.1 Introduction

We have already discussed about the idea of chemical modulation of the perovskite structure subjected to change in temperature and percentage variation of Sb, Bi. $\text{Cs}_3\text{M}_2\text{X}_9$ ($\text{M} = \text{Sb, Bi}$; $\text{X} = \text{Cl, Br}$) perovskites exist in two different crystal structures, namely trigonal and orthorhombic [1,2]. It has been seen that for a temperature of 85°C and at $x=1(\text{Cs}_3\text{Sb}_x\text{Bi}_{2-x}\text{Cl}_9)$, the trigonal phase is predominant. We also see there is an existence of orthorhombic phase as well. Moreover, we have found that it is comparatively easier to vary the particle size of this material in a controlled fashion by controlling its stoichiometric ratio and temperature. Recently, Pradhan et al. [3] have synthesized mixture of trigonal and orthorhombic phases of $\text{Cs}_3\text{Sb}_2\text{Cl}_9$ nanocrystals by tuning the precursors and ligands. Yao et al. [4] have synthesized a series of $\text{A}_3\text{M}_2\text{X}_9$ ($\text{A} = \text{CH}_3\text{NH}_3$, Cs, Rb ; $\text{M} = \text{Sb, Bi}$; $\text{X} = \text{Cl, Br, I}$) perovskite nanocrystals with Bi substitution at Sb site. Methylammonium lead halide perovskites appeared as groundbreaking solar cell absorbers with comparable power conversion efficiency to that of traditional silicon solar cell materials. However, these compounds suffer drawback for practical application in large scale because of the toxicity [5-7] of lead as well as their poor stability upon light, heat, and atmospheric moisture [8,9]. Instead of three divalent cations (Pb^{2+}) in a halide perovskite ($\text{Cs}_3\text{Pb}_3\text{X}_9$; $\text{X} = \text{halide}$) two trivalent cations (M^{3+}) can be substituted and led to a new perovskite of formula $\text{Cs}_3(\text{M}^{3+})_2\text{X}_9$ [10,11]. These kinds of substitution further lead to improve photovoltaic performance with an added advantage of choosing earth abundant and non-toxic elements. Hence, these materials could be further studied for the improvement in carrier mobility, better light absorption capability, manipulating their band gaps as well as stability with the variation of different elements at various sites of the material.

4.2 Experimental details

4.2.1 Synthesis

Cs₃SbBiCl₉ powder was synthesized employing novel colloidal route of synthesis. We have modified the reported synthesis process to achieve the simplest way to get the same material. Firstly, CsCl ($\geq 99\%$), SbCl₃ ($\geq 99.5\%$), BiCl₃ ($\geq 99.99\%$), HCl, C₂H₅OH (99%; Thermo Fischer) are taken without any further purification. In a typical synthesis, stoichiometric amount of CsCl, SbCl₃, and BiCl₃ were taken inside a single beaker and 30 ml of concentrated HCl was added into it. The beaker containing the solution mixture was placed in an oil bath and kept at 85°C temperature with continuous stirring for 45 minutes. The solubility of precursors in the reaction mixture gives indication towards the different phase formation. For example, after 45 min of continuous stirring at 85°C, a turbid solution of Cs₃SbBiCl₉ was obtained. After that the solution is mixed with polar solvent of ethanol. Then it is kept in a centrifuge tube.

Centrifugation is done at 5000 rpm for 10 minutes to separate liquid and solid phases apart. Once centrifugation is done, the solid phase is separated and kept the tube inside vacuum oven at 75°C for overnight. Finally, a pale-yellow colored powder sample is obtained. Further analysis is done afterwards.

Chemical reaction: $3\text{CsCl} + \text{SbCl}_3 + \text{BiCl}_3 = \text{Cs}_3\text{SbBiCl}_9$

4.2.2 Characterization

The synthesized samples were characterized in order to find out crystallinity of the sample by the X-ray diffraction (XRD; Bruker, D-8 Advance) with the Cu K α radiation having wavelength $\lambda = 1.5406 \text{ \AA}$. The morphological insights of the synthesized sample was studied by field emission scanning electron microscope (FESEM, Hitachi, S-4800). The elemental composition or percentage of all occupied elements was analyzed by energy dispersive X-ray analysis (EDAX).

4.3 Result and discussion

4.3.1 Structural and compositional study

XRD pattern of the prepared sample of $\text{Cs}_3\text{SbBiCl}_9$ shows different peak intensities for different 2θ values. It shows good crystallinity of the sample are in well agreement with JCPDS. XRD patterns of $\text{Cs}_3\text{SbBiCl}_9$ powder sample is shown in **Fig.4.1**

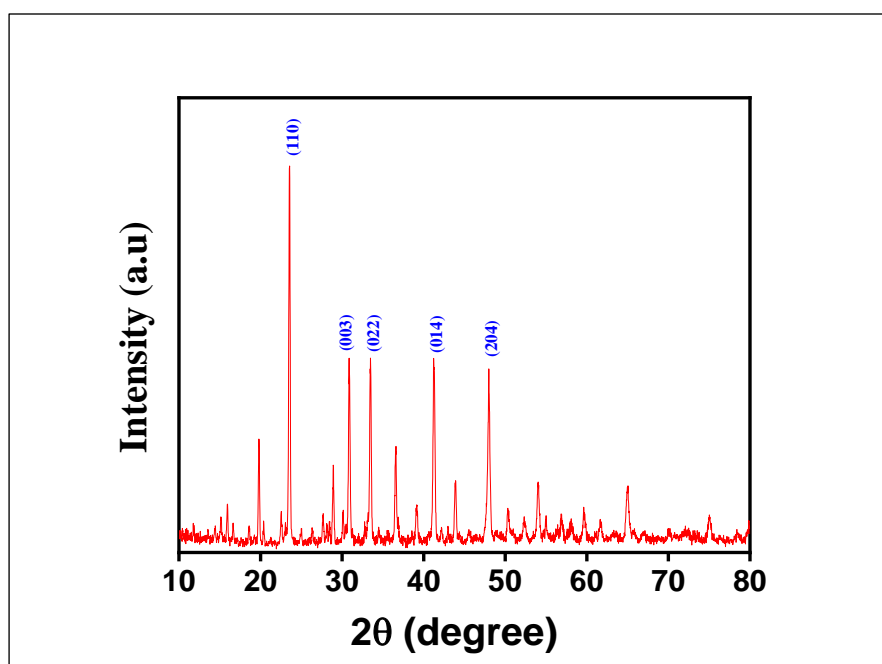


Fig.4.1- XRD patterns of $\text{Cs}_3\text{SbBiCl}_9$ powder sample

XRD pattern shows pick intensities at (110), (003), (022), (014), (204) plans for the corresponding values of 2θ are 23.54° , 30.85° , 33.46° , 41.31° , 48.1° respectively. The crystallite size were calculated from the XRD data using following Scherrer's equation.

$$D = 0.9 \lambda / \beta \cos\theta$$

Where, D is the crystallite size, λ be the wave length, θ be the bragg's angle and β is the full width half maximum (FWHM).

We have calculated the crystallite size $D = 68 \text{ nm}$

Rietvelt refinement analysis

The Rietvelt output profile shows that trigonal and orthorhombic phases are present in the sample. Also shows the calculated intensity (I_c), observed intensity (I_o) and residual intensity ($I_o - I_c$) of the coexisting phases of the sample. Trigonal phase is more predominant in this case.

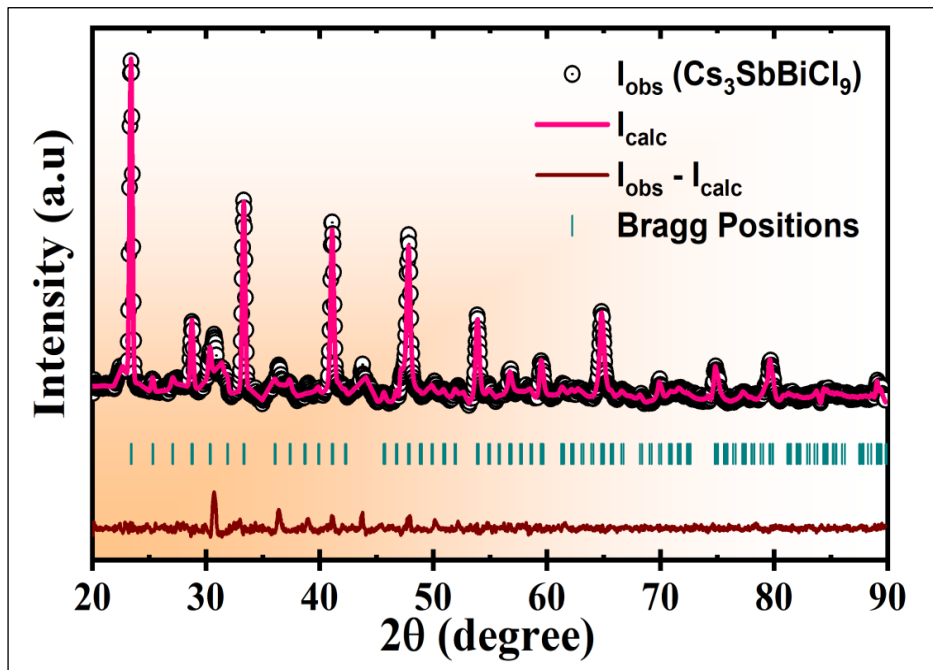


Fig. 4.2- Rietvelt refinement analysis shows the existence of both orthorhombic and trigonal phases.

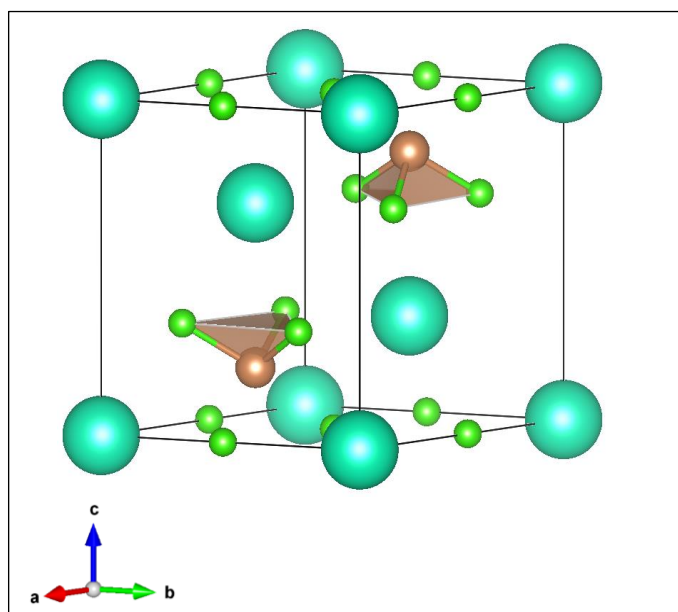


Fig. 4.3- Cs, Sb/ Bi, Cl atoms are arranged to form a unit cell in Rietvelt analysis

At the corner of the unit cell Cesium (Cs) atoms are present. Antimony/ bismuth (Sb/ Bi) is bonded with three neighboring chlorine (Cl) atoms. Forming a dual structure comprises of trigonal and orthorhombic 3D lattice structure.

4.3.2 Morphological studies

FESEM images were observed and are presented of $\text{Cs}_3\text{SbBiCl}_9$ perovskite sample. Images show a stone like 3D morphology or hexagon like structure. The average length of the stone like structure is approximately $10\mu\text{m}$.

We also studied energy dispersive X-ray analysis, where, we have seen the elementary compositions of all participated elements, mostly on the surface of the sample from its intensity versus binding energy plot. Stoichiometric ratio also could be known from this information. A FESEM image is shown below along with the EDAX data. 'Cl' present in the sample is approximately 63%, 'Cs' is about 21% and rest will be shared almost equally by Bi and Sb atoms.

The stoichiometric ratio is Cs: Sb : Bi : Cl = 3 : 1 : 1 : 9.

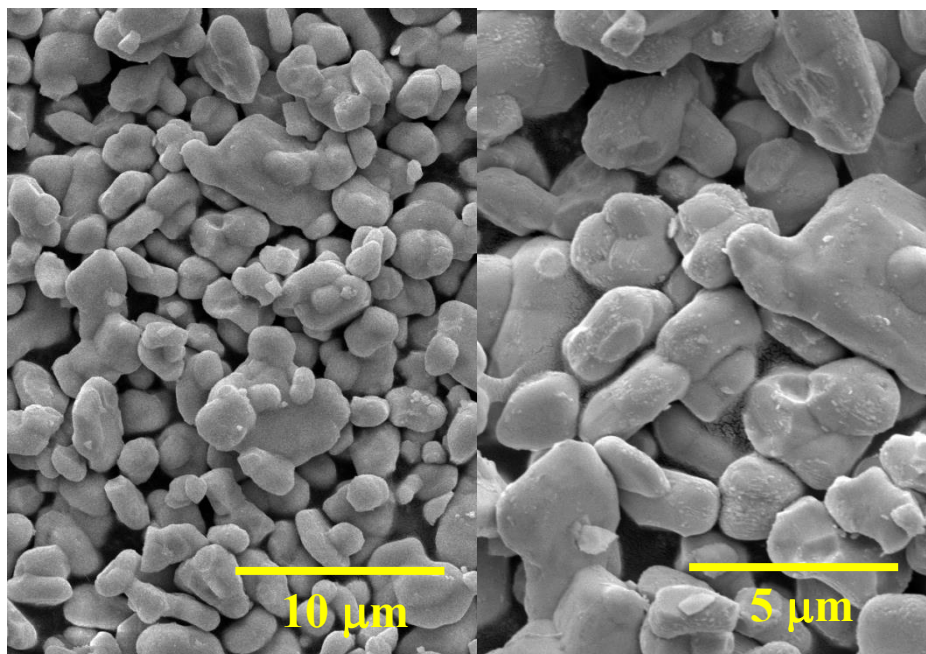


Fig.4.4- There are two FESEM images of different scaling factor (10 μm and 5 μm).

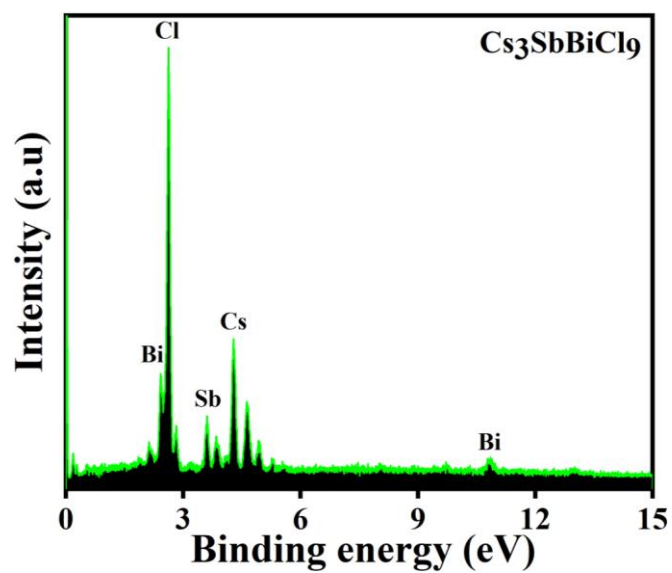


Fig.4.5- Energy dispersive X-ray analysis for the investigation of elementary composition.

4.4 Conclusion

Utilizing the possibilities of nanotechnology, a material with attractive electrical, catalytic properties are accomplished. Nanocrystalline $\text{Cs}_3\text{SbBiCl}_9$ powders were prepared via low cost colloidal synthesis method at different with precursor solutions leading to low dimensional particle size. The XRD study showed that the proper dual phase of the material has been formed and the constituent elements. The FESEM studies show the morphological view of the materials. EDAX analysis show the proper elementary compositions of different elements. The good electrical property with tunable bandgaps have been also observed with $\text{Cs}_3\text{SbBiCl}_9$. So, these properties can tell that it is a leading candidate to be used in nanogenerator application, self-powered devices, high-performance solid-state batteries, photodetectors and solar cells.

References

- [1] A.N. Banerjee, S. Kundoo, K.K. Chattopadhyay, *Thin Solid Films* 440 (2003) 5-10.
- [2] A.N. Banerjee, R. Maity, K.K. Chattopadhyay, *Mater. Lett.* 58 (2003) 10-13.
- [3] A.N. Banerjee, C.K. Ghosh, K.K. Chattopadhyay, *Sol. Energy Mater. Sol. Cells* 89 (2005)75-83.
- [4] R. Laskowski, N.E. Christensen, P. Blaha, B. Palanivel, *Phys. Rev. B* 79 (2009) 165209/1-7.
- [5] M. Snure, A. Tiwari, *Appl. Phys. Lett.* 91 (2007) 092123/1-3.
- [6] X. Nie, Su-H. Wei, S.B. Zhang, *Phys. Rev. Lett.* 88 (2002)066405/1-4.
- [7] Gallet, C. and F. Pellisier. 1997*J. Chern. Ecol.* 23:2401-2412.[8] Harwood,C.S. and I. Gibson. 1997. *179:301-309.*
- [8] Hameed, A., Gombac, V., Montini, T., Graziani, M., &Fornasiero, P. (2009). *ChemicalPhysics Letters*, 472(4), 212-216.
- [9] Umadevi, M., & Christy, A. J. (2013). *SpectrochimicaActa Part A: Molecular and Biomolecular Spectroscopy*, 109, 133-137.
- [10]Abdelhamid, Hani Nasser..Vol. 832.*Trans Tech Publications*, 2015.
- [10] Y. Wang, M. Trenary, *Chem. Mater.* 5 (1993) 199-205.
- [11] L. Vayssieres, *Int. J. Nanotechnology*1 (2004) 1-41
- [12] Sonawane, N. B., Baviskar, P. K., Ahire, R. R., &Sankapal, B. R. (2017).

Chapter -5

Cs₃SbBiCl₉ and PVDF composite thin film preparation, characterization

Introduction

Mechanical energy is the most abundant energy in our daily life and has attracted many researchers' interests to convert mechanical energy to available energy. Due to flexibility, simple preparation and cost-effectiveness, polymer-based piezoelectric nanogenerator (PENG) play an important role in the development of self-powered electronics [1, 2], pressure sensors [3], energy supply [4,5] and medical monitoring [6]. Poly (vinylidene fluoride) (PVDF) and its copolymers with high-voltage electrical response and excellent mechanical properties have been widely used in the variety of energy conversion applications [7-12]. The piezoelectric phase of PVDF (electroactive β phase) can be transferred by mechanical stretching or external electrode polarization at high electric field temperatures. However, the additional polarization process can easily lead to structural damage and electrical breakdown. Electrospinning technology is a method that not only creating an electrostatic force to fabricate fibers in high electric field induction, but also promoting the growth of polarized β phases through polarization. Therefore, the additional mechanical stretching and electron polarization steps are critically required for the electro-spun film. In addition, adding external fillers such as perovskites [13], graphene oxide [14], carbon nanotubes [15-17], montmorillonite [18] and metal salts [19,20] was also a good way to improve the β phase transformation through interfacial interaction between the matrix and the filler.

Except the β phase content, the transfer of induced charge also had a direct effect on the electrical power generation properties. Graphene, halide perovskite, metals and carbon nanotubes were usually used as conductive fillers to improve the rapid transfer of charge [21-23]. Shi, et al [24] fabricated the barium titanate (BT), perovskite and PVDF comprised nanocomposites by drop casting. In this chapter we will discuss that how composite thin films are being prepared and can be used as nanogenerator.

5.1 Experimental details:

- **Preparation of PVDF- $\text{Cs}_3\text{SbBiCl}_9$ composite thin film**

In this process, 1.5 gm PVDF pallets were added in acetone (12 ml) and DMF (8 ml) mixture. Afterwards, as synthesized $\text{Cs}_3\text{SbBiCl}_9$ with different concentration (3, 4, 5, 6 and 7 wt% (w/v)) was added to the above solution and stirred for 2 h at 70°C. A semi-yellow colored, homogeneous solution was prepared which was further solution drop casted on pre-cleaned glass slides.

These coated substrates were kept in vacuum at 75°C for over-night. Thereafter, films were taken off from the glasses and used for device fabrication and various characterizations. A schematic of film preparation and collection is shown in fig. 5.1.

Depending on the concentration of $\text{Cs}_3\text{SbBiCl}_9$ in the composite film we have labeled the as prepared samples as PVDF (PVDF film only), PVSB 3, PVSB 4, PVSB 5, PVSB 6 and PVSB 7 where, attached numeric with PVSB denotes weight percentage of $\text{Cs}_3\text{SbBiCl}_9$ in the composite.

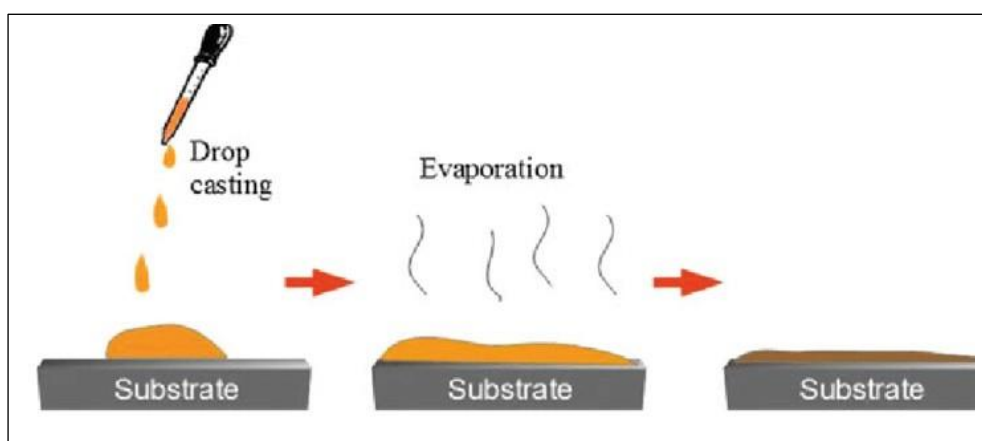


Fig. 5.1- $\text{Cs}_3\text{SbBiCl}_9$ Perovskite and PVDF composite drop casted over glass substrate.

5.2 Result and discussion:

5.2.1 Structural analysis by XRD

Diffraction peaks which indicate good crystallinity of the prepared thin films are shown respectively. There are 5 composite thin films which subjected to XRD analysis. We have seen some peaks are matching with the perovskite itself, which signifies the existence of the sample material into PVDF polymer. Bare PVDF does not have those peaks. The XRD peaks of composites (PVSB 3, PVSB 4, PVSB 5, PVSB 6, PVSB 7) were assigned to be arising due to reflections from (110), (003), planes which concludes the proper phase formation of the given composite. On the other hand, intensity of the aforesaid peaks in PVSB 5 is decreased and few new peaks appeared. A semi-electroactive phase. Peaks in XRD profile of PVSB 5 at 19.8° and 23.8° are associated with the (002) and (110) plane of electroactive β -phase

The proper phase formation and good degree of crystallinity is important for nanogenerator. Good crystallinity obtained in our sample ensured that initially. However, there are further scopes of improvement of crystallinity of $\text{Cs}_3\text{SbBiCl}_9$ samples which may additionally contribute to enhance electroactive β phase for mechanical energy harvesting application, charge storage performance.

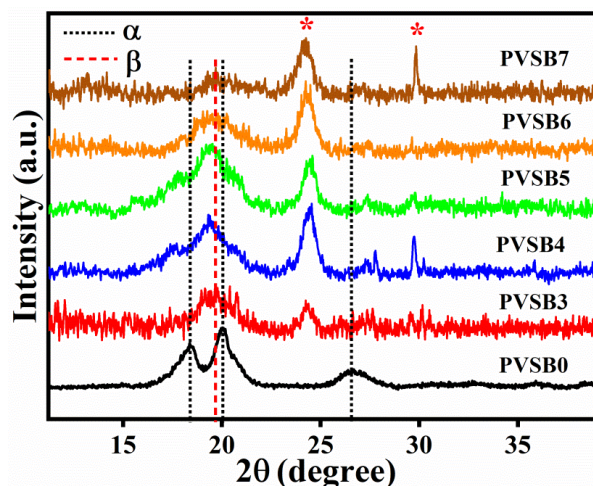


Fig. 5.2- XRD analysis of PVDF- $\text{Cs}_3\text{SbBiCl}_9$ composite thin films

5.2.2 Morphological analysis by FESEM:

Morphological nature of composite thin films of a few weight percentage values were observed at different magnification. At higher magnification it was found that the film has a porous structure. FESEM images clearly show that in few regions, nanoparticles agglomerate. Though, most of the area of surface show good porosity. Which means these composite films have larger effective surface area. Surface to volume ratio increased.

This property is very important for the fact that higher that effective surface area higher will be the functionality. Many other materials could be incorporated onto it for more applications The flake natures in any semiconductor nanostructure may contribute positively in charge storage performance, the higher value of effective surface area, as can be found in flake like structures, can essentially offer higher area for charge movement and therefore charges can be retained there for a longer time.

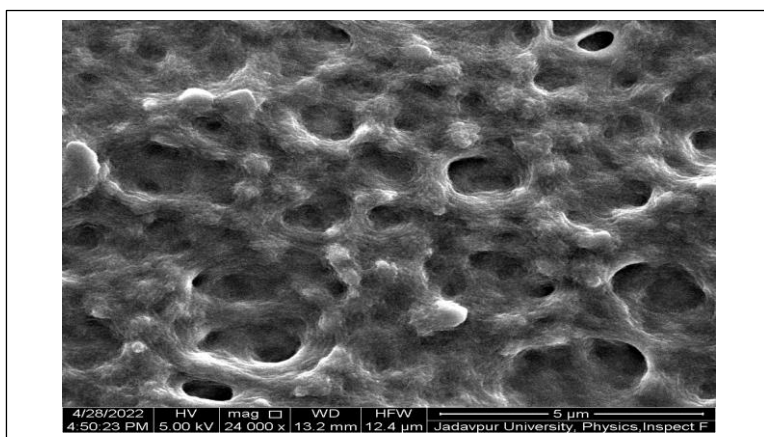


Fig. 5.3- Porous and flaky structure of PVDF- $\text{Cs}_3\text{SbBiCl}_9$ composite thin film.

5.2.3 Electroactive β phase analysis by FTIR:

FTIR spectroscopy was carried out for all the samples to identify the crystalline phase presence and the results are shown in Fig. 5.4. Characteristics vibrational band at 1150, 976, 796, 764, 613, 532 cm. assigned to non-polar α phase of PVDF whereas semi-polar γ phase related characteristics band appeared at 1234, 812 cm. % of $\text{Cs}_3\text{SbBiCl}_9$. While the intensity of the band at 1279 cm enhance progressively with the increase of $\text{Cs}_3\text{SbBiCl}_9$ content in composite films up to 5 wt %. Superimposed band nearly 840 cm^{-1} is used to determine the electroactive phase content in composite. Electroactive phase content (F_{EA}) in all composites are determined with the help of this equation

$$F_{EA} = \frac{A_{840}}{\frac{K_{840}}{K_{764}} A_{764} + A_{840}} \times 100\%$$

where A_{764} and A_{840} are the absorbance intensity at 764 and 840 cm respectively. K_{764} and K_{840} are absorption coefficient corresponding to the aforesaid bands with values 6.1×10^4 and $7.7 \times 10^4 \text{ cm}^2/\text{mol}$. Electroactive phase content in the samples increased with perovskite loading increment up to 5 wt% and thereafter it is decreased (fig. 5.6). Maximum percentage of FEA is achieved for PVSb 5 which is nearly 90% whereas the same for PVDF film is as low as 39%. For facile comparison we have tabulated β phase content in the samples against perovskite constitution in Table. Interaction between positive surface charge of $\text{Cs}_3\text{SbBiCl}_9$ and $-\text{CH}_2\text{-CF}_2-$ dipole in PVDF chain enhances the electroactive phase percentage in the composites. Due to low perovskite content in PVSb 3 and PVSb 4, such interaction is nominal which in turn limits the conversion of β phase from α phase. With moderately high loading of perovskite (PVSb 5), filler distributed throughout the polymer matrix uniformly and

more interaction is resulted. Filler concentration beyond 5 wt%, created agglomeration of perovskite within the polymer matrix and surface charge interaction with the dipole is lowered. Interfacial interaction of $\text{Cs}_3\text{SbBiCl}_9$ and PVDF dipole is obvious from the FTIR spectrum within the range 3050–2960 cm^{-1} in fig. 5.5.

Absorption peaks at ~ 2980 and ~ 3023 cm^{-1} related to symmetric and asymmetric $-\text{CH}_2-$ bond stretching which have great meaning in electroactive phase formation in interfacial interaction. Shifting of these peaks is only accounted due to the disruption of vibrational bands. Both peaks are blue shifted for the composite films as compared PVDF only which suggests interaction between the perovskite and PVDF dipole. Increase in interfacial interactions enhanced the effective mass of $-\text{CH}_2$ molecules which further lead to a decrease in vibrational frequency of the aforesaid. Such interaction acts a source of damping. Damping constant is related with angular frequency of $-\text{CH}_2$ stretching vibration dipole under damped and undamped condition. Assessed values of damping constants are found to increase with the perovskite content in the film. It is noteworthy to mention here that F_{EA} and damping constant follow the similar kind of behavior with perovskite loading. Such analogous behavior suggests a direct relationship between β phase formation in PVDF matrix as a consequence of interaction of the dipoles with $\text{Cs}_3\text{SbBiCl}_9$.

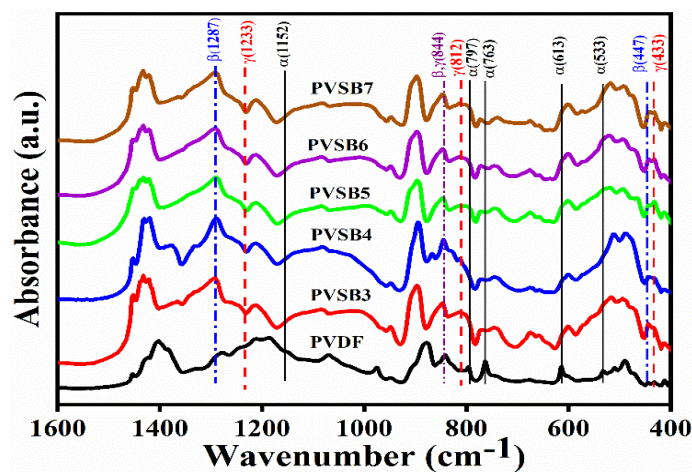


Fig. 5.4 – FTIR spectra in the range of 1600 cm^{-1} to 400 cm^{-1}

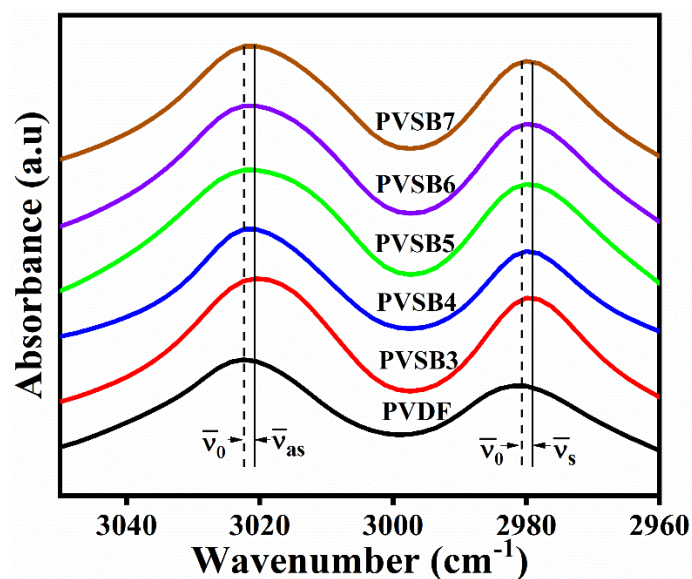


Fig. 5.5 - FTIR spectra in the range of 3050 cm⁻¹ to 2960 cm⁻¹ showing symmetric and asymmetric stretching.

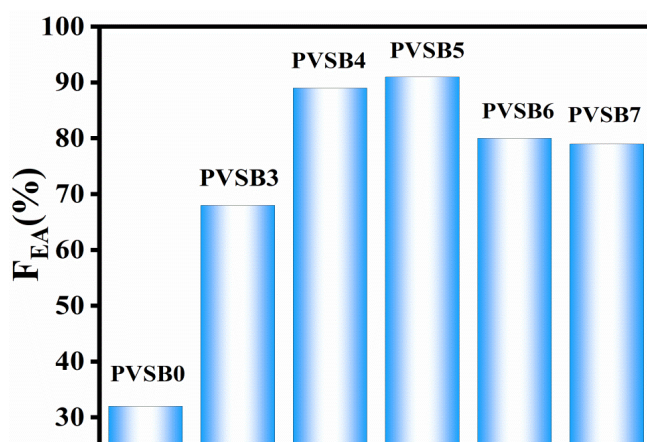


Fig. 5.6 – Electroactive phase for different weight percentage of Cs₃SbBiCl₉ showing maximum β phase content at 5 wt%.

5.2.3 Dielectric measurement analysis by impedance analyzer

The basic principle of impedance analyzer and LCR meter have already been discussed in the previous chapter. Here we will discuss the nature of dielectric constant and loss tangent of those composite thin films. When these are subjected to high frequency, how their dielectric property changed. We would also discuss about the dielectric loss during

the change in frequency.

All these properties are important in order to behave as a piezoelectric material. How they are polarized or, their electric dipoles get separated during change in frequency. Composite thin films are tested in an impedance analyzer machine. We will find out their behavior when exposed to high frequency. These parameters are important from the electrical point of view.

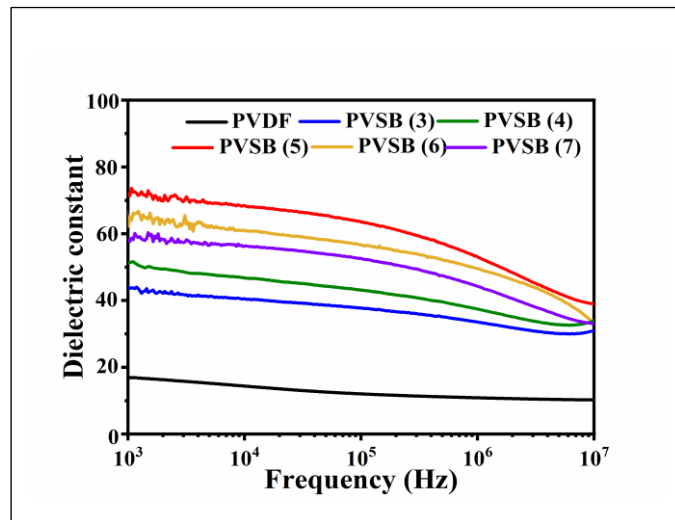


Fig .5.7- Frequency versus dielectric constant curve for composite films

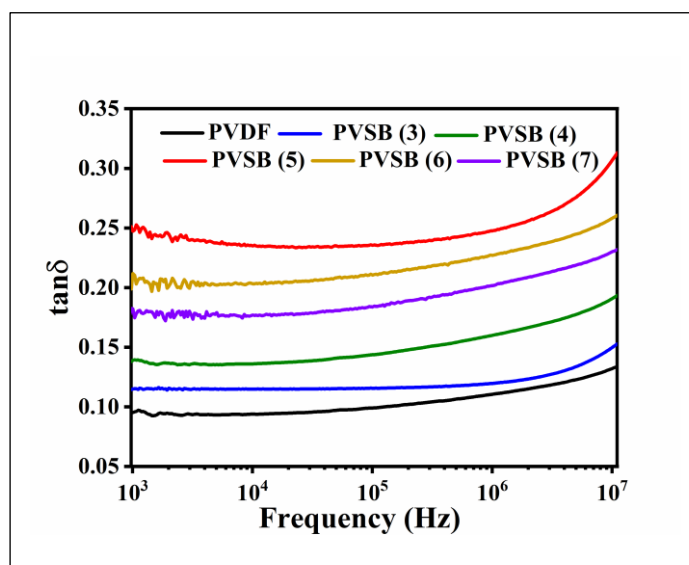


Fig. 5.8- Frequency versus dielectric loss tangent curve for composite thin films

5.3 Conclusion

In conclusion, we have reported on an all-inorganic cesium antimony chloride perovskite NCs using colloidal synthesis route. Uniform stone like structures of several micron length and aspect ratio-controlled NRs have been obtained by tuning precursors and temperature. Morphology analysis by FESEM shows a porous structure which can be functionalized to make bio sensor, gas sensor, etc. The FTIR study shows that these thin films are capable of enhancing the electroactive beta phase of PVDF polymer. Hence these can be used as piezoelectric material for bio mechanical energy harvester. Our work provides an approach for the fabrication of environmentally friendly analogous $\text{Cs}_3\text{SbBiX}_9$ ($\text{X} = \text{Br}, \text{Cl}, \text{I}$) perovskites NCs. These new NCs may find applications in perovskite NCs based devices such photodetectors, active material for solar cells, batteries and nanogenerators etc.

References

- [5] A.N. Banerjee, S. Kundoo, K.K. Chattopadhyay, *Thin Solid Films* 440 (2003) 5-10.
- [6] A.N. Banerjee, R. Maity, K.K. Chattopadhyay, *Mater. Lett.* 58 (2003) 10-13.
- [7] A.N. Banerjee, C.K. Ghosh, K.K. Chattopadhyay, *Sol. Energy Mater. Sol. Cells* 89 (2005)75-83.
- [8] R. Laskowski, N.E. Christensen, P. Blaha, B. Palanivel, *Phys. Rev. B* 79 (2009) 165209/1-7.
- [5] M. Snure, A. Tiwari, *Appl. Phys. Lett.* 91 (2007) 092123/1-3.
- [6] X. Nie, Su-H. Wei, S.B. Zhang, *Phys. Rev. Lett.* 88 (2002)066405/1-4.
- [11] Gallet, C. and F. Pellisier. 1997*J. Chern. Ecol.* 23:2401-2412.[8] Harwood,C.S. and I. Gibson. 1997. *179:301-309.*

- [12] Hameed, A., Gombac, V., Montini, T., Graziani, M., & Fornasiero, P. (2009). *Chemical Physics Letters*, 472(4), 212-216.
- [13] Umadevi, M., & Christy, A. J. (2013). *Spectrochimica Acta Part A: Molecular and Biomolecular Spectroscopy*, 109, 133-137.
- [14] Abdelhamid, Hani Nasser..Vol. 832. Trans Tech Publications, 2015.
- [13] Y. Wang, M. Trenary, *Chem. Mater.* 5 (1993) 199-205.
- [14] L. Vayssieres, *Int. J. Nanotechnology* 1 (2004) 1-41
- [15] Sonawane, N. B., Baviskar, P. K., Ahire, R. R., & Sankapal, B. R. (2017). *Materials Chemistry and Physics* 191 (2017) 168e172
- [16] B. Saha, S. Das and K.K. Chattopadhyay, *Solar Energy Mat. & Sol. Cell* 91(2007) \p.1692-1697.

Chapter -6

**Device fabrication of composite thin films,
subjected to different bio-mechanical
movements, results**

6.1 Introduction

In order to study the piezoelectric response, we have prepared several kind nanogenerators using PVSb 3, PVSb 4, PVSb 5, PVSb 6 and PVSb 7 composite and coined them as PNG 3, PNG 4, PNG 5, PNG 6 and PNG 7 where PNG stands for piezoelectric nanogenerator and the attached numeric with that denotes weight percentage of $\text{Cs}_3\text{SbBiCl}_9$ in the composite. For facile comparison we have also fabricated another device using PVDF only. Mechanical energy-harvesting features of all the devices were examined (A. Sultana et al.[1]) without any electrical poling treatment. Piezo response of all the nanogenerators was analyzed by applying repeated hammering with hand (with gloves) in vertical direction (Suvankar Mondal et al. [2]). Both voltage and current output is found to be higher for the PNGs as compared to the bare PVDF nanogenerator (bare PVDF delivered an open circuit voltage (V_{oc}) 15 V and short circuit current (I_{sc}) 1.18 μA . Among all PNGs, PNG 5 showed maximum output voltage 273 V with a short circuit current of 15.45 μA .

6.2 Experimental details

6.2.1 Device fabrication

- Composite thin films are fabricated over PET substrate to enable them to be extremely flexible. So that it could be bent and stretch by the application of mechanical stress, or any kind of bio mechanical pressure.
- That PET substrate is first wrapped by aluminum foil. 'Al' would be used as electrode material for our case.
- Then thin films are placed over that PET substrate and attached with any insulating tape.
- After that the expose surface is also covered be aluminium foil.

- Basically, we have to make a capacitor like sandwiched structure so that, the electric dipoles can be separated in presence of external pressure onto it.

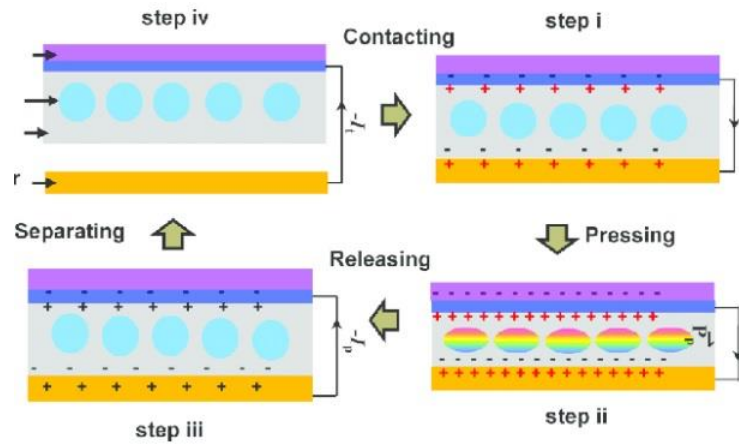


Fig. 6.1- Electric dipole alignment of PENG under mechanical stress.

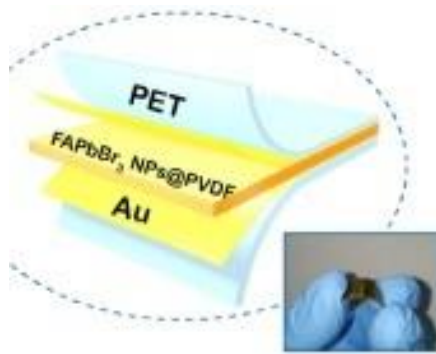


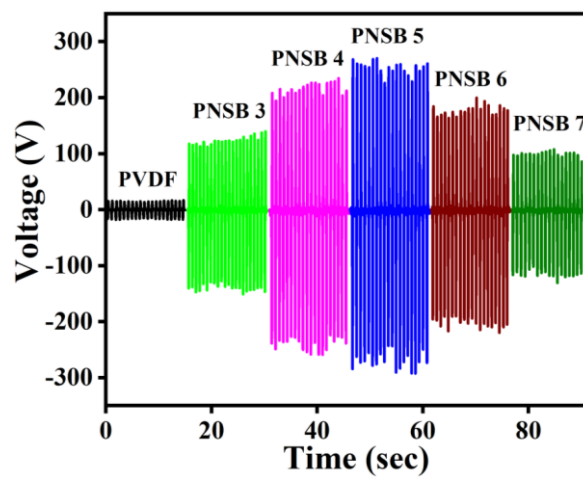
Fig. 6.2- Capacitor like sandwiched structure of PENG

6.3 Result and discussion

6.3.1 Analysis of different electrical parameters

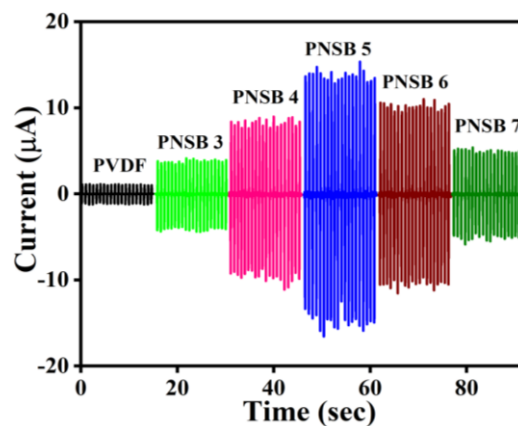
1. Voltage under mechanical pressure on PENG

Maximum open circuit voltage of 273 V is obtained at 5 wt% of the sample material.



2. Current under mechanical pressure on PENG in presence of resistive load

Maximum short circuit current under mechanical pressure is $15.45\mu\text{A}$.



3. Forward and reverse connection of PENG

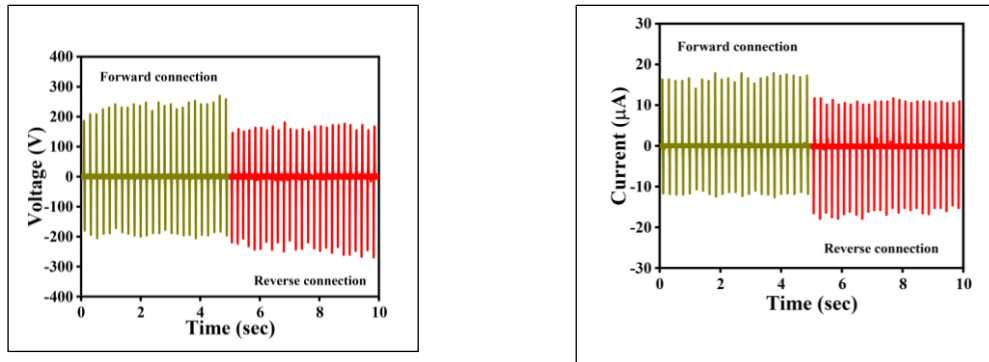


Fig 6.3 - Performance of PENGs for forward and reverse connection observed in CRO

4. Performance of PENGs under different load resistance

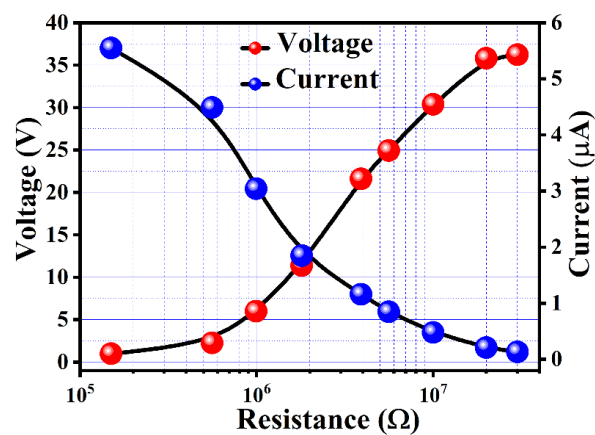


Fig. 6.4- Voltages and currents under different values of load resistance

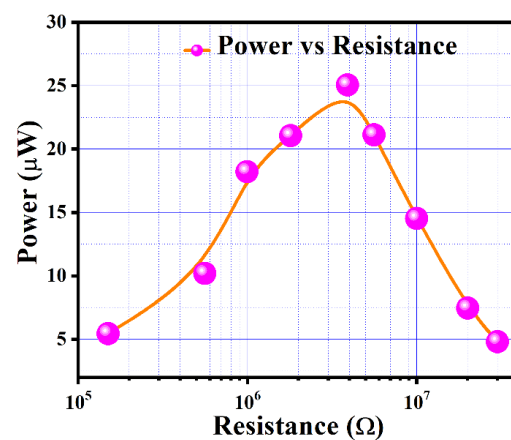


Fig. 6.5 - Power versus resistance curve under different resistance

5. Rectified voltage output of PENG

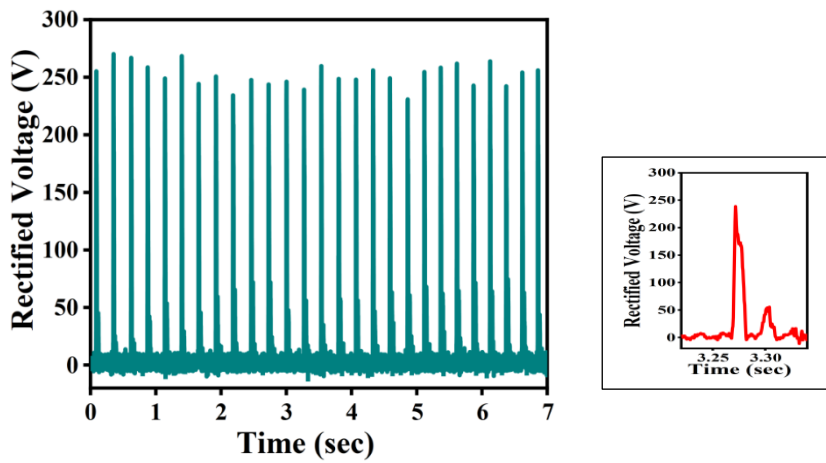


Fig. 6.6- Rectified voltage and one of the half-wave is shown here.

6. Capacitor charging by PENGs

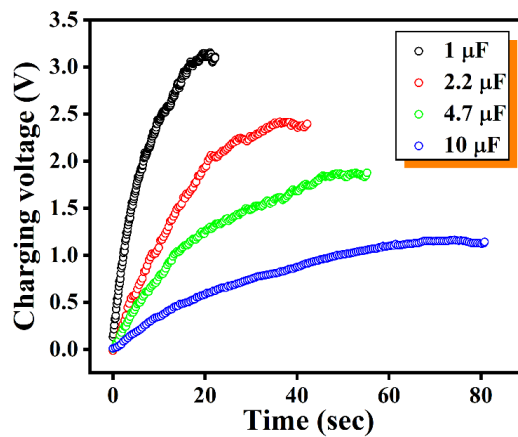


Fig. 6.7- Charging of capacitors having different capacitance value

7. Lighting up LEDs by PENG

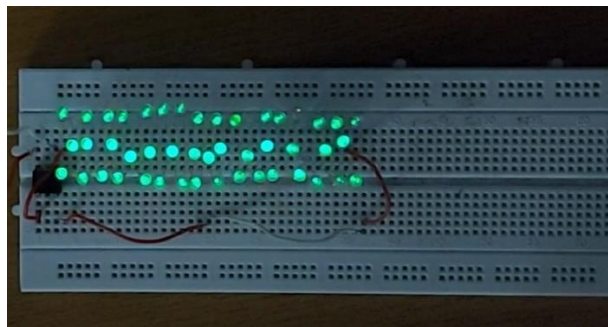
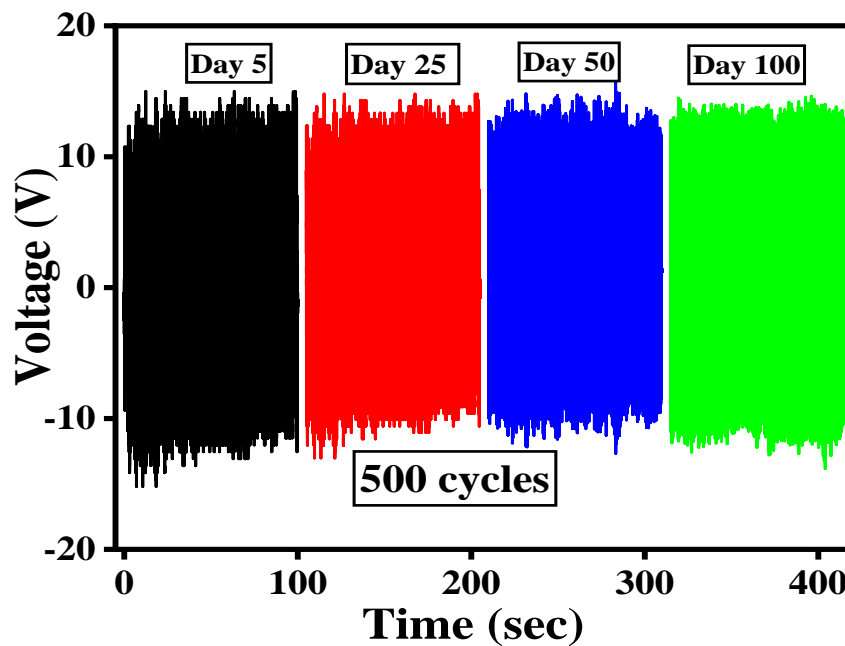


Fig. 6.8- Glowing of several LEDs by PENG.

8. Long cycle analysis of composite thin films:

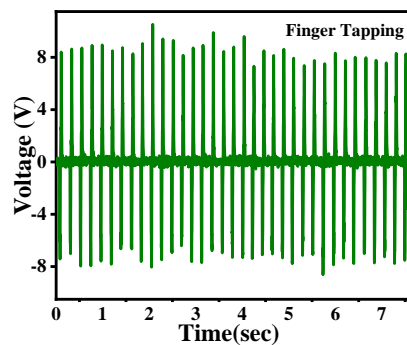
The performance of this perovskite nanogenerator has been analyzed in regular intervals to see their stability performance. It has been seen after 100 days also they are capable of giving equally good performance. The long cycle data was taken for over hundred seconds under continuous pressure exerting on the device.



6.3.2 Analysis of different bio-mechanical movements: Energy harvesting

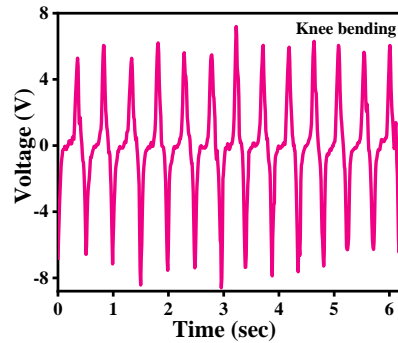
- **Finger tapping:**

As we can see the average voltage on tapping by finger is about 8-10 volts



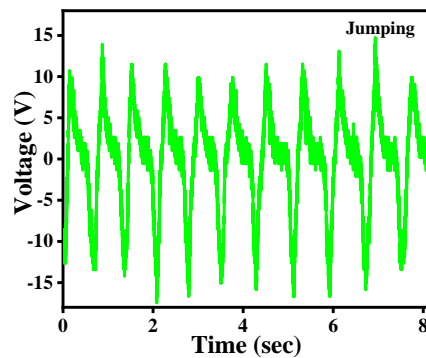
- **Knee bending**

PENGs when placed under knee joint, a simple bending could give a voltage up to 7-8 volts.



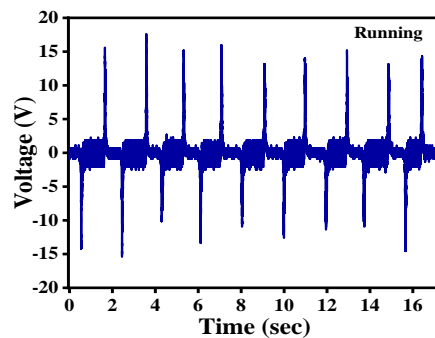
- **Jumping**

During Jumping, if PENGs could be connected underneath our feet it could produce a very high voltage.



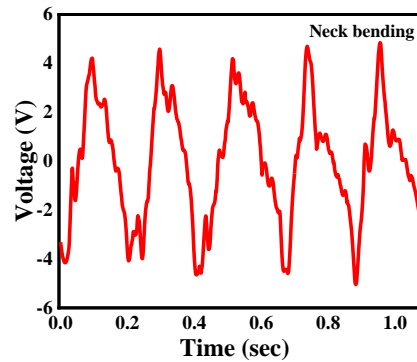
- **Running**

PENGs subjected to pressure like, running, walking could produce electricity.



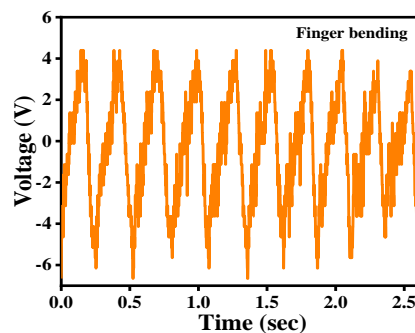
- **Neck Bending**

Electrical energy is being produced by PENGs under simple bending of neck, may be during exercise.



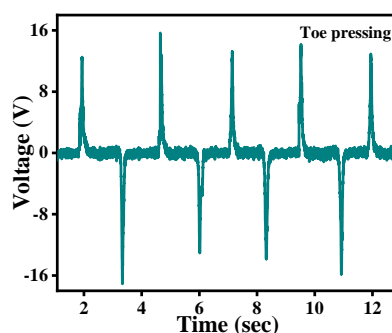
- **Finger Bending**

PENGs placed under palm, fingers, only a movement or bending would produce electricity.



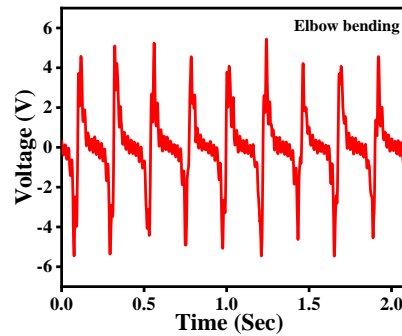
- **Toe pressing**

Nanogenerators attached under the toes would produce electricity during walking or, any kind of movements.



- **Elbow bending**

A simple bending of elbow could generate voltage if a PENG is attached with the elbow.



- **COMSOL simulation**

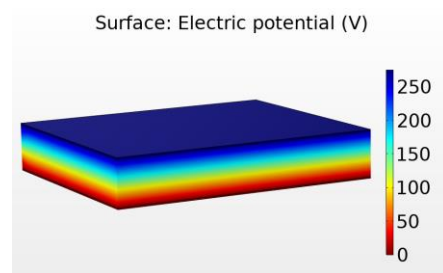


Fig.6.9 - COMSOL simulation showing electrical potential distribution of PENGs.

References

- [1] Sultana A, Alam MM, Middya TR, Mandal D. A pyroelectric generator as a self-powered temperature sensor for sustainable thermal energy harvesting from waste heat and human body heat. *Applied Energy*. 2018 Jul 1;221:299-307.
- [2] Mondal S, Paul T, Maiti S, Das BK, Chattopadhyay KK. Human motion interactive mechanical energy harvester based on all inorganic perovskite-PVDF. *Nano Energy*. 2020 Aug 1;74:104870

Chapter 7

Conclusion and scope for future work

7. Conclusion and scope for future work

7.1 Conclusion

In summary, we have discussed the fundamental concepts about perovskite materials. The study also shows how these materials are modified by different methods to work efficiently and in environmentally viable manner. We have studied specifically about lead free double perovskite synthesis by cost-effective colloidal route, characterization techniques and applications in biomechanical energy conversion. We have also learned about the composite preparation with PVDF polymer. We have seen how the electroactive beta phase could be enhanced and make it possible to be used as a piezoelectric nanogenerator. Performance of some perovskites like, CsPbI_3 , Cs_2SnI_6 , MAPbI_3 , $\text{Cs}_2\text{AgBiBr}_6$ have been studied during the course of literature surveying. Metal halide double perovskite has been chosen as novel material based on some interesting properties like, tunable band gap, high carrier diffusion length, narrow direct band gap, high electron mobility etc. It has been seen in the earlier chapters that group 5A metalloids (Bi, Sb) are very versatile elements. These elements can replace Pb. As we know that Pb is a toxic element, it is necessary to replace it with other non-toxic elements for better compatibility and safety. These trivalent metalloids can serve the purpose. Here in this course, we have synthesized $\text{Cs}_3\text{SbBiCl}_9$ perovskite. It contains trigonal and orthorhombic lattice structure. The interesting fact is that we could tune structural phase by varying the quantities of Bi and Sb, also by changing the temperature. Different structure would show different optimized properties as we have learned during this study.

Finally, we made $\text{Cs}_3\text{SbBiCl}_9$ – PVDF composite thin films. Based on that we have learned and modified some easy procedure to fabricate nanogenerator. Which has produced excellent result in energy harvesting through simple human body movement. The precision, sensitivity, cost effectiveness could make them a promising biomechanical energy harvester in the near future. We have also observed in the earlier paper that these perovskites also exhibit good

optoelectronic properties due to their high absorption co-efficient. So, there is a possibility that these metal halide double perovskites could work as a hybrid material for multipurpose applications like piezoelectric energy harvesting, light detection and in hybrid devices and bridge the way towards self-powered photodetector application.

This whole Chapter has been designed to get acquainted with this new technology along with the execution and what could be the future of this technology.

7.2 Scope for future

Nanotechnology refers any technology on a nanoscale that has applications in the real world. Nanotechnology encompasses the production and application of physical, chemical, and biological systems at scales starting from individual atoms or molecules to submicron dimensions, as well as the integration of the resulting nanostructures into larger systems. Nano technology is likely to have a profound impact on our economy and society in the early 21st century, comparable to that of semiconductor technology, information technology or, molecular biology. Science and technology research in nanotechnology promises breakthroughs in areas such as materials and manufacturing, nanoelectronics, medicine and healthcare, energy, biotechnology, information technology, and national security. It is widely felt that nanotechnology will be the next Industrial Revolution.

- This perovskite-polymer composite is very promising in terms of their excellent optoelectronics and piezo-electrical property. These enable researchers to develop piezo-photoelectronic devices.
- We could make use of these materials to develop hybrid devices, which incorporate photo active sensor as well as piezo-sensor.
- Large scale production of these perovskite materials has been a challenge since past. So, we need to find some easy route of synthesis. Here, we have used colloidal route of synthesis, which considered to be a promising

alternative to other tedious processes.

- Abundancy of precursor salts has been a challenge. In order to achieve a large-scale industrial production of highly efficient PENGs we need to search some easily available precursors. Which can be optimized to get the same level of performance.
- Researchers also need to find out some rudimentary technique of fabrication PENG devices. Our unique and easy fabrication method could be a breakthrough in this field.